Energy Conversion and Management 276 (2023) 116533

Contents lists available at ScienceDirect

Energy Conversion and Management

journal homepage: www.elsevier.com/locate/enconman

Thermoeconomic comparison of a molten carbonate fuel cell and a solid oxide fuel cell system coupled with a micro gas turbine as hybrid plants

Juan Pedro Pérez-Trujillo [a,b,*], Francisco Elizalde-Blancas [c], Massimiliano Della Pietra [d], Dulce María Silva-Mosqueda [c], Juan Manuel García Guendulain [b], Stephen J. McPhail [e]

[a] Applied Electrochemistry, Department of Chemical Engineering, KTH - Royal Institute of Technology, SE-100 44 Stockholm, Sweden
[b] Industrial Technology Division, Polytechnic University of Querétaro, 76240 El Marqués, Querétaro, Mexico
[c] Department of Mechanical Engineering, DICIS, University of Guanajuato, 36885 Salamanca, México
[d] ENEA R. C. Casaccia, TERIN-PSU-ABI, Via Anguillarese 301, 00123 Rome, Italy
[e] Kiwa Cermet, Business Sector Energy, Via Cadriano 23, 40057 Bologna, Italy

A B S T R A C T

This study presents a comparative evaluation of Molten Carbonate Fuel Cell (MCFC) and Solid Oxide Fuel cell (SOFC) stacks coupled with a micro gas turbine (MGT). For the analysis, it is assumed that the fuel supply to the stacks is constant in all the analyzed conditions. The components of the system have been sized using the first law of thermodynamics to meet the thermal conditions required to maintain fuel cell stack operation, while an exergetic analysis has been implemented in order to assess the components in terms of irreversibilities. Furthermore, an economic analysis to estimate the Levelized Cost of Electricity (LCOE) has been carried out to indicate the most feasible option between the two analyzed systems. The capacity of the fuel cell stacks is 500kW$_{dc}$ operating at 350 kPa and 600 °C/650 °C. The results indicate that MCFC stacks are more efficient than SOFC stacks, but are considerably more expensive. Nevertheless, the SOFC/MGT system has a global efficiency higher than that of the MCFC/MGT; also its Total Capital Investment (TCI) is 2.5–3.5 times lower, thus making the SOFC/MGT coupling more attractive. The only product considered coming out from the systems to determine the LCOE is electricity. The LCOE for the SOFC/MGT system is 0.339–0.402$/kWh and for the MCFC/MGT is 0.875–0.897$/kWh, which for both configurations is still higher than the current electricity prices. One aspect that increases the investment and consequently the LCOE is the high cost of the stacks and their replacements which is around 19 % and 10 % of the total Purchased Equipment Cost (PEC) for MCFC and SOFC stacks, respectively.

1. Introduction

The coupling between gas turbines and high-temperature fuel cells has been widely studied in the last two decades [1–4]. The hybrid system consists of a high-temperature fuel cell stack that could be either a MCFC or a SOFC as the main cycle, and a gas turbine (GT) or a steam turbine (ST) as a bottoming cycle operated with the remaining energy from the main cycle. High-temperature fuel cells are preferred in stationary power generation systems because of their capacity to manage different fuels, as well as their ability to tolerate compounds like carbon monoxide considered as a poison in low-temperature fuel cells. The exhaust gases coming out from low-temperature fuel cells have too low a content of thermal energy to drive another conventional system like steam or gas turbines. The reported operative conditions of hybrid systems are very diverse in the literature and depend on the application that they are designed for.

A hybrid SOFC/GT/ST system is analyzed in [1], where the efficiency and cost of systems ranging in size from 1.5 to 10MWe are evaluated. It was found that the system with the higher power installed was the most efficient. This is attributed to the fact that the efficiency in steam turbines improves with size. The range of SOFC stack pressures tested was from 8 to 10 bar and the SOFC stack temperature was evaluated from 950 to 1100 K, obtaining an average efficiency of the system of 68.4 %.

A SOFC/GT system within a net power plant of 500 kW is tested in [2]. The system was operated with methane, methanol or kerosene in four system layouts. The results show that with methanol a lower efficiency is obtained but an attractive economic performance. The operation with methane shows highest efficiency, 64.5 % for a fuel cell stack pressure and temperature of 4 bar and 800 °C, respectively.

A thermodynamic, economic and environmental evaluation of SOFC/GT and SOFC/Internal combustion Engine (ICE) is studied in [5]. The SOFC stack lifetime is assumed to be 40,000 h, with the stack replacement every 5 years. The operative temperature and pressure of the SOFC stack are 850 °C and 1 bar. The net electrical efficiency of the SOFC/GT hybrid is 57.64 % and the LCOE is 0.3202$/kWh.

A MCFC/GT system is analyzed in [3] using first- and second-law thermodynamics. The results show that the catalytic burner is the

* Corresponding author.
E-mail addresses: jppt@kth.se, jp.pereztrujillo@hotmail.com (J.P. Pérez-Trujillo).

https://doi.org/10.1016/j.enconman.2022.116533
Received 23 August 2022; Received in revised form 31 October 2022; Accepted 27 November 2022
Available online 7 December 2022

Nomenclature

B	Exergy, kJ
b	Specific exergy, kJ/kg
C	Heat capacity, kW/K
C_r	Heat capacity ratio, -
E^0	Reversible open circuit voltage, V
F	Faraday constant, 96485.33C/mol
h	Enthalpy, kJ/kg
$h^0_{f.298}$	Enthalpy of formation at 298 K, kJ/kg
I	Current, A
i_{eff}	Average annual effective discount rate, %
$\dot{m}$	Mass flow rate, kg/s
n	Number of electrons involved in the electrochemical reaction
$\dot{n}$	Molar flow rate, kmol/s
NTU	Number of heat transfer units, –
P	Pressure, kPa
$\dot{Q}$	Rate of heat transfer, kW
R	Universal Gas Constant, 8.314 kJ/kmol K
s	Specific entropy, kJ/kg
T	Temperature, K
U	Utilization factor, %
UA	Overall heat transfer coefficient, W/K
V	Voltage, V
$\dot{W}$	Power, kW
x	Mass fraction, –
y	Mole fraction, –
Z	Cost, $

Greek symbols

β	Pressure ratio, -
ε	Effectiveness, –
η	Efficiency, %
$\dot{\sigma}$	Entropy production rate, kJ/K

Subscripts and superscripts

a	Air
ac	Alternating current
act	Activation overpotentials
c	Cold side
ch	Chemical
con	Concentration overpotentials
CV	Control volume
d	Exergy destruction
dc	Direct current
e	Exit
f	Fuel
fe	Fuel electrode
g	Combustion gases
h	Hot side
hf	High frequency current
i	Inlet
j	Stoichiometric coefficient of product
k	Stoichiometric coefficient of reactant
L	Levelized
lf	Low frequency current
$LMTD$	logarithmic Mean Temperature Difference
max	Maximum
min	Minimum
n	System lifetime
oe	Oxygen electrode
ohm	Ohmic overpotentials
P	Products
ph	Physical
R	Reactants
ref	Reference state
w	Water
0	Dead state

Acronyms and abbreviations

AFC	Auxiliary Fuel Compressor
BPV	Value of by-products
C	Compressor
CC	Carrying Charges
CHP	Combined Heat and Power
CRF	Capital-recovery factor
ECO	Economizer
EVA	Evaporator
FC	Fuel compressor or Fuel Costs
FCI	Fixed Capital Investment
FCS	Fuel Cell Stack
FF	Fuel cost
G	Electrical Generator
GT	Gas Turbine
HRSG	Heat Recovery Steam Generator
HX	Heat Exchanger/Pre-heater
ICE	Internal Combustion Engine
IEA	Internal Energy Agency
INV	Inverter
LCOE	Levelized Cost of Electricity
MCFC	Molten Carbonate Fuel Cell
MGT	Micro Gas Turbine
MPQ	Main Product Quantity
MPUC	Main Product Unit Cost
O&M	Operation and Maintenance
OMC	Operation and Maintenance Costs
P	Pump
PEC	Purchased equipment cost
RC	Recompressor
REF	Reformer
RG	Regenerator
ST	Steam Turbine
SOFC	Solid Oxide Fuel Cell
SUP	Superheater
T	Turbine
TCI	Total Capital Investment
TDC	Total Direct Costs
TNCI	Total Net Capital Investment
TRR	Total revenue requirement

component with the highest irreversibilities. Besides, the maximum work output of the MCFC is 314.3 kW and the overall energy and exergy efficiencies achieved were 42.89 % and 37.75 %, respectively, when the fuel cell operating temperature is 650 °C and the pressure is 4 bar.

A MCFC/MGT configuration is analyzed by Iora et al. [6] where the operative conditions of the micro gas turbine are used to regulate and improve the performance of the MCFC stack at partial loads. The sizing of the components is carried out in off-dessign conditions respecting the matching of the gas-turbine, the part-load behavior of the fuel cell, and the rest of components. The fuel cell stack is representative of the 500 kW Ansaldo Twinstack or 2TW and the micro gas turbine was scaled based on the reference curves of a Bownman TG60. The results show how acting in sequency on 1) the turbine shaft speed, 2) the air-to-fuel ratio, 3) the bypass of a fraction of air across the cell cathode, and 4)

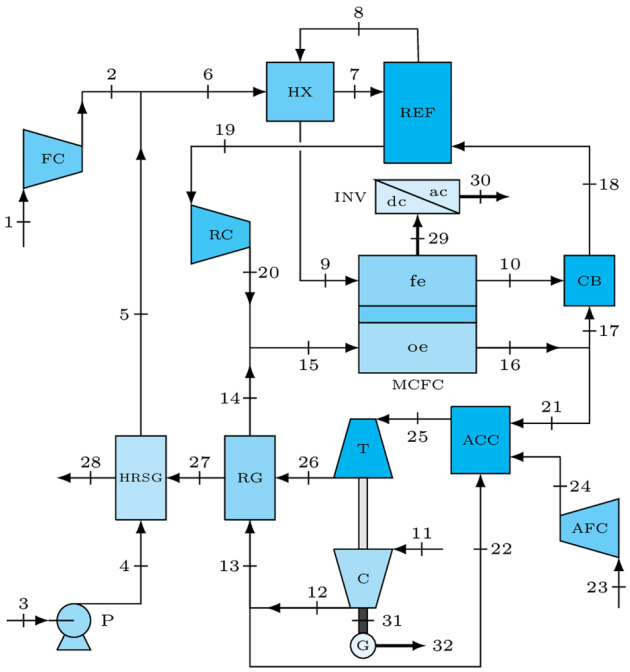

Fig. 1. MCFC/MGT hybrid system configuration. Adapted from [6].

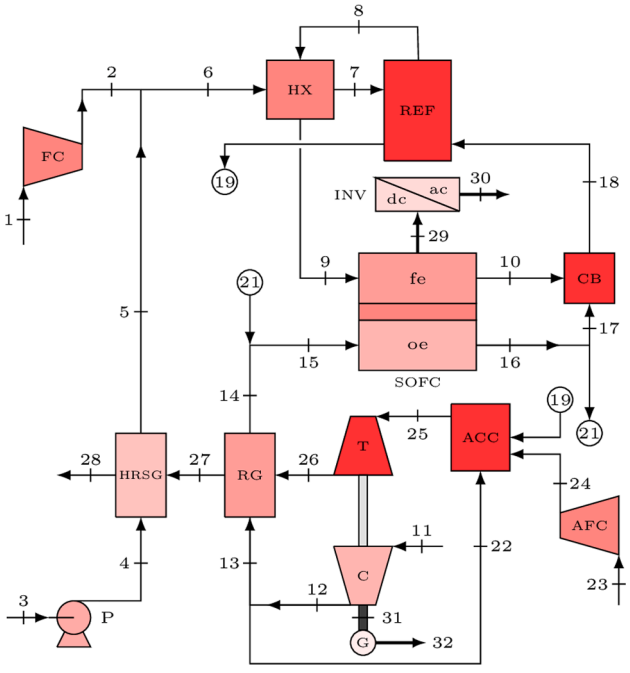

Fig. 2. SOFC hybrid system configuration.

the fuel utilization, help to regulate effectively the plant power output.

In order to increase the use of renewable energies and reduce the dependence of hydrocarbons, renewable alternatives need to be economically and environmentally competitive with respect to current options. In the SOFC/GT or MCFC/GT system the most expensive component is the fuel cell stack. The reported cost of the MCFC stack is $1327/kW [7] in 2020, almost 4.7 times more expensive than the SOFC stack with an estimated cost of $282.9/kW [5]. The reduction in the cost of stack manufacturing can be achieved by increasing the production as Scataglini [8] claimed, with a target value of $238/kW, that is much lower than the installed cost for steam turbines, $430–1100/kW [9]. The cost trends for different fuel cells is presented in [10] considering the annual produced units and their impact on the cost of combined-heat-and-power configurations.

Thermoeconomic analyses are useful to get a more realistic approach of a thermal system while evaluating economic and thermal feasibility. In combination with exergetic analyses it is possible to identify the components with the higher irreversibilities, that in terms of efficiency represent the main losses, or translated into running costs, the most expensive operative parts. Thermoeconomic analyses also allow to compare between different configurations which is the most competitive [5,7], e.g. the comparison of three different supercritical carbon dioxide bottoming cycles using the exhaust gases of an MCFC stand-alone system carried out in [7], where a lower LCOE was found for all three analyzed cases compared to the current price of electricity. Nevertheless, in the economic analysis the cost of the fuel cell stack replacements during the lifetime of the system is not indicated, i.e., only one stack is considered for the 20 years of the overall lifetime of the plant whereas stack lifetime is about 5 years. This parameter is important because it indicates that the LCOE is being underestimated and could jeopardize the maintenance of the system and the real payback period. This assumption is also found in other thermoeconomic analyses [11,12]. Nevertheless, there are others analyses where the lifetime of the fuel cell stack is considered correctly, obtaining more comprehensive values of LCOE [5,13,14].

Ryu et al. calculate the LCOE using a stand-alone MCFC with respect to four bottoming configurations to utilize the exhaust gases of a MCFC that include combined heat and power, supercritical CO_2 Recompression Brayton cycle, supercritical CO_2 Reheat Recompression Brayton cycle, and supercritical CO_2 Brayton Rankine Cascade cycle. The simulated exhaust gas conditions for a MCFC of 2800 kW were considered to evaluate the bottoming configurations. The LCOE ranges between 0.1715$/kWh to 0.1733$/kWh.

The MCFC can be coupled with traditional power plant systems to capture CO_2 as indicated in [15,16]. Desideri et al. [15] indicate that around 62 % of the CO_2 contented in the exhaust gases from a cogeneration power plant can be separated with a purity of 82 %. Samanta and Ghosh [16] show that using MCFC to separate the CO_2 of the exhausted gases of a 250 MW can help to increase the plant capacity by 6.7 % and the net plant efficiency by 7.43 %. The CO_2 emissions can be reduced around 90 % although the LCOE of the system rises from 0.057$/kWh to 0.108$/kWh. Nevertheless, the utility of the CO_2 is not taken into account to determine the LCOE.

Moshin et al. [14] evaluate a carbon capture and utilization case for a 500 MW power plant using a MCFC system to separate the CO2. It is assumed that 97 % of the CO2 is sequestrated. After CO2 is sequestrated it is reduced to obtain different products that include: carbon monoxide, formic acid, methanol, ethylene, ethanol and *n*-propanol. The cost of derived products and three scenarios (conservative, baseline, and optimistic) are considered in calculating the LCOE, that ranges from 0.020 $/kWh to 0.225$/kWh depending on the product analyzed, where CO is the option that most decreases the LCOE.

Accordingly, it is quite challenging to make a comparison between different systems and indicate which one is more efficient when operative conditions are not the same. It certainly will be easier when the systems have the same reference. Thus, the aim of this work is to compare for the first time the two types of high-temperature fuel cells, SOFC and MCFC, coupled with a GT under the same operative conditions in order to analyze which one is more efficient and with the lowest LCOE. The reference condition considered is keeping the same energy content in the fuel supplied to the fuel cell stack. The auxiliary components were sized at 600 °C and 650 °C to fulfil the reference conditions, their energetic matching and the constraints of the first and second law of thermodynamics. Additionally, the locations with higher entropy generation are determined by using an exergetic analysis, and finally we conclude with an economic analysis to compare the total capital investment and the levelized cost of electricity to determine the best option purely based on the considered benchmark conditions of the stack.

Table 1
Design parameters of the MCFC and SOFC systems.

	600 °C		650 °C	
	MCFC	SOFC	MCFC	SOFC
Fuel compressor (FC)				
β_{FC}[-]	3.632		3.632	
$\dot{m}_{FC}$[kg/s]	0.021		0.021	
η_{FC}[%]	80.000		80.000	
Recompressor (RC)				
β_{RC}[-]	1.020	–	1.020	–
$\dot{m}_{RC}$[kg/s]	3.076	–	2.903	–
η_{RC}[%]	60.000	–	60.000	–
Pre-heater (HX)				
UA_{HX}(W/K)	104.445	107.102	62.011	61.958
$\dot{m}_{HX,h}$[kg/s]	0.106		0.106	
$\dot{m}_{HX,c}$[kg/s]	0.106		0.106	
$\Delta P_{HX,h}$[%]	1.108		1.108	
$\Delta P_{HX,c}$[%]	1.902		1.902	
Pump (P)				
β_{RC}[-]	4.698		4.698	
$\dot{m}_{RC}$[kg/s]	0.085		0.085	
η_{RC}[%]	80.000		80.000	
Heat Recovery Steam Generator (HRSG)				
$\dot{m}_{HRSG,h}$[kg/s]	1.328	1.296	1.559	0.919
$\dot{m}_{HRSG,c}$[kg/s]	0.085		0.085	
$\Delta P_{HRSG,h}$[%]	2.572		2.572	
$\Delta P_{HRSG,c}$[%]	22.689		22.689	
Economizer (ECO)				
UA_{ECO}(W/K)	627.240	833.439	1128.302	921.689
Evaporator (EVA)				
UA_{EVA}(W/K)	2756.072	3840.358	4086.139	3066.71
Super heater (SUP)				
UA_{SUP}(W/K)	56.440	53.897	60.027	45.985
Turbine (T)				
β_T[-]	3.222		2.974	3.222
$\dot{m}_T$[kg/s]	1.328	1.296	1.559	0.919
η_T[%]	85.700		85.700	
Compressor (C)				
β_C[-]	3.523		3.523	
$\dot{m}_C$[kg/s]	1.220	1.189	1.450	0.813
η_C[%]	79.500		79.500	
Reformer (REF)				
UA_{REF}(W/K)	4234.704	2585.32	3219.79	1593.925
$\dot{m}_{REF,h}$[kg/s]	3.076	0.985	2.903	0.781
$\dot{m}_{REF,c}$[kg/s]	0.106		0.106	
$\Delta P_{REF,h}$[%]	1.153		1.153	
$\Delta P_{REF,c}$[%]	1.108		1.108	
Regenerator (RG)				
UA_{RG}(W/K)	4028.231	3277.932	13655.404	2166.220
$\dot{m}_{RG,h}$[kg/s]	1.328	1296	1.559	0.919
$\dot{m}_{RG,c}$[kg/s]	0.146	0.309	0.203	0.138
$\Delta P_{RG,h}$[%]	3.704		11.111	3.704
$\Delta P_{RG,c}$[%]	1.961	1.681	1.681	
Fuel Cell Stack (FCS)				
$\dot{W}_{dc}$[kW]	500.000		500.000	
V[V]	0.714	0.688	0.755	0.672
U_f[%]	69.257	74.047	65.502	73.674
ΔP_{fe}[%]	0.286		0.286	
ΔP_{oe}[%]	0.286		0.286	

2. System configuration

A hybrid system consisting of a high-temperature fuel cell and a MGT as a bottoming system is analyzed. Two different configurations are analyzed by changing uniquely the type of fuel cell, MCFC or SOFC. The capacity of the fuel cell stacks is defined to be 500kW$_{dc}$, because this power is equivalent to small modules that can be used in commercial combined heat and power (CHP) applications or as assembly systems to reach higher capacities. Since the direct current obtained from the fuel cell stacks cannot be directed to the grid without conditioning, e.g. frequency regulation, it is necessary to use an inverter (INV) to convert the output from direct current to alternating current. Nevertheless, the conversion of electrical current in the inverter produces losses that decrease the target power. To compensate those losses a MGT is coupled to the system providing the difference of power. Fig. 1 shows the configuration for the MCFC/MGT system taken from [6], with the addition of the inverter in the fuel cell stack and the electrical generator (G) in the MGT. Both devices are going to be considered in the thermoeconomic analysis.

Fig. 2 shows the SOFC/MGT system configuration which has the same auxiliaries as the MCFC/MGT system, with the only difference that the re-compressor (RC) is not included in the SOFC/MGT system. Instead, the combustion gases leaving the reformer (REF) are sent directly to the auxiliary combustion chamber (ACC). Besides, a percentage of the air leaving the oxygen electrode is mixed with the air supplied by the MGT in order to decrease the demand on the air compressor (C). This change has been implemented because SOFCs do not require carbon dioxide in the oxygen electrode to carry out the electrochemical reaction. Besides, there is evidence that the water content and carbon dioxide in the oxygen electrode could increase the degradation of the cell, promoting diverse phenomena that depend on the nature of the oxygen electrode [17,18]. Thus, there is the possibility to either send only air to the oxygen electrode or to recirculate the combustion gases. In this work, it has been opted to analyze the first option to avoid that carbon dioxide or water reache the oxygen electrode.

In order to make an appropriate comparison of the two systems, both configurations are technically the same, as well as the operating conditions like pressure, temperature and flow rates of the fuel in stream 1 and water in stream 3, which are maintained constant in all the analyzed cases. Two cell temperature values are studied, 600 °C and 650 °C, maintaining the pressure of the fuel cell stack at 350 kPa. More details of the design parameters are shown in Table 1. In the case of the MCFC/MGT configuration, the reference data were taken from [6] and recalculated until satisfying the 500kW$_{ac}$ by using the electrochemical model presented in Section 3. Concerning the SOFC/MGT configuration, the operating conditions for each piece of equipment have been calculated to satisfy the configuration shown in Fig. 2 and the power indicated.

The main assumptions to obtain the design conditions and the sizing of the components in all the cases are listed below:

- The amount of fuel supplied to the fuel cell stack, stream 1, and water, stream 3, are constant in all cases in order to have the same reference condition.
- All the fuel is oxidized in the catalytic burner and the auxiliary combustion chamber.
- Pressure and temperature of the streams entering the anode are the design conditions of the fuel cell stack, 350 kPa and 600/650 °C, respectively.
- The reference case is based on the conditions published in [6] to evaluate a MCFC/MGT at 600 °C and 350 kPa. The design of this case was compared with the values reported in [6] obtaining mainly pressure drops in the components, pressure points, efficiencies of electric generator and inverter, reformed gas composition, and bypass of the outlet cathodic gas flow rate.
- The air-to-fuel-ratio was kept constant as $\dot{m}_{15}/\dot{m}_9 = 39.2054$, as well as the steam-to-carbon ratio, $\dot{m}_4/\dot{m}_1 = 4.04$.
- A constraint between the fuel cell stack, catalytic burner, reformer, heat exchanger and recompressor was set to calculate the interactions of these components until the changes in composition and temperature satisfy the power of the stack, 500 kW. This constraint was set using a while-loop maintaining constant the pressure drop of the components, the efficiency of the catalytic burner and recompressor, until the relative error in the mole fraction of the CO_2 and O_2 coming out from the cathode was less than 1×10^{-6}.
- In the SOFC/MGT configuration, the recompressor is not required because the CO_2 formed in the catalytic burner is not needed in the cathode. The combustion gases are directed to the axuliary combustion chamber. The stream coming out from the cathode is mixed

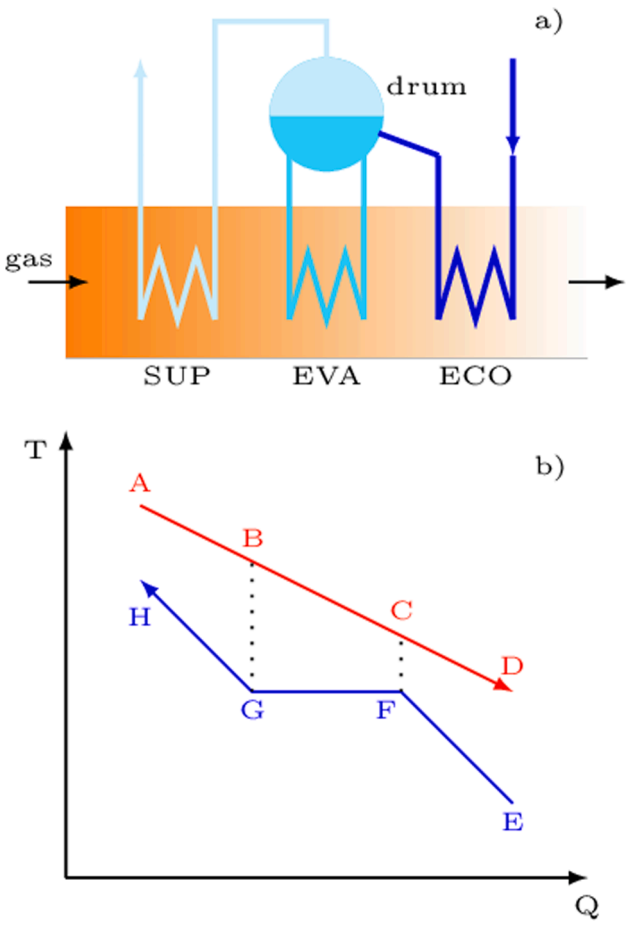

Fig. 3. Representation of the HRSG. Adapted from [6].

Table 2
Geometrical assumptions for the electrochemical models of the fuel cell stacks.

	MCFC [19,25]	SOFC [5,26]
Stack module capacity	250 kW_{dc}	100 kW_{dc}
Cells per module	292	500
Active area per cell, m^2	0.72	0.05
Type of cell	Planar	Planar and anode supported
Fuel electrode		
Thickness, m	0.7×10^{-3}	4.05×10^{-4}
Porosity, %	51.9	39
Tortuosity	2	5.5
Oxygen electrode		
Thickness, m	0.9×10^{-3}	1.5×10^{-5}
Porosity, %	67	55
Tortuosity	2	1.7

with new air, stream 13, to be enriched in oxygen before entering the cathode again. The amount of air bypassed in stream 22 is calculated to meet the thermal conditions in the HRSG and RG.

- A counterflow configuration is considered for the design of the heat exchangers and the $NTU-\varepsilon$ method is used for sizing.
- Most of the equipment is considered to run adiabatically except the reformer and the fuel cell stacks that are placed together in an adiabatic container to facilitate the heat transfer between the two components [19].
- The minimum terminal temperature difference in the regenerator is contrained to be no less than 2.5 °C [20].
- No pinch-point or approach-point constraint or optimization was set in the Heat Recovery Steam Generator (HRSG) [21]. Nevertheless, it was ensured that gases temperatures were always higher than the temperature of water to have heat transfer from the combustion gases to water according to Fig. 3.
- Entropy production is always positive.

Table 3
Energy and exergy balance equations per component.

	Energy	Exergy
FCS	$\dot{m}_9 h_9 + \dot{m}_{15} h_{15} = \dot{m}_{10} h_{10} + \dot{m}_{16} h_{16} + \dot{W}_{FCS} + \dot{Q}_{FCS}$	$\dot{m}_9 h_9 + \dot{m}_{15} h_{15} = \dot{m}_{10} h_{10} + \dot{m}_{16} h_{16} + \dot{W}_{FCS} + \dot{Q}_{FCS} + \dot{B}_d$
T	$\dot{m}_{25} h_{25} = \dot{W}_T + \dot{m}_{26} h_{26}$	$\dot{m}_{25} h_{25} = \dot{W}_T + \dot{m}_{26} h_{26} + \dot{B}_d$
C	$\dot{m}_{11} h_{11} + \dot{W}_C = \dot{m}_{12} h_{12}$	$\dot{m}_{11} h_{11} + \dot{W}_C = \dot{m}_{12} h_{12} + \dot{B}_d$
RC	$\dot{m}_{19} h_{19} + \dot{W}_{RC} = \dot{m}_{20} h_{20}$	$\dot{m}_{19} h_{19} + \dot{W}_{RC} = \dot{m}_{20} h_{20} + \dot{B}_d$
FC	$\dot{m}_1 h_1 + \dot{W}_{FC} = \dot{m}_2 h_2$	$\dot{m}_1 h_1 + \dot{W}_{FC} = \dot{m}_2 h_2 + \dot{B}_d$
AFC	$\dot{m}_{23} h_{23} + \dot{W}_{AFC} = \dot{m}_{24} h_{24}$	$\dot{m}_{23} h_{23} + \dot{W}_{AFC} = \dot{m}_{24} h_{24} + \dot{B}_d$
P	$\dot{m}_3 h_3 + \dot{W}_P = \dot{m}_4 h_4$	$\dot{m}_3 h_3 + \dot{W}_P = \dot{m}_4 h_4 + \dot{B}_d$
REF	$\dot{m}_{18} h_{18} + \dot{m}_7 h_7 + \dot{Q}_{REF} = \dot{m}_{19} h_{19} + \dot{m}_8 h_8$	$\dot{m}_{18} h_{18} + \dot{m}_7 h_7 + \dot{Q}_{REF} = \dot{m}_{19} h_{19} + \dot{m}_8 h_8 + \dot{B}_d$
CB	$\dot{m}_{17} h_{17} + \dot{m}_{10} h_{10} = \dot{m}_{18} h_{18} + \dot{Q}_{CB}$	$\dot{m}_{17} h_{17} + \dot{m}_{10} h_{10} = \dot{m}_{18} h_{18} + \dot{Q}_{CB} + \dot{B}_d$
ACC	$\dot{m}_{21} h_{21} + \dot{m}_{22} h_{22} = \dot{m}_{24} h_{24} + \dot{m}_{25} h_{25}$	$\dot{m}_{21} h_{21} + \dot{m}_{22} h_{22} = \dot{m}_{24} h_{24} + \dot{m}_{25} h_{25} + \dot{B}_d$
RG	$\dot{m}_{13} h_{13} + \dot{m}_{26} h_{26} = \dot{m}_{14} h_{14} + \dot{m}_{27} h_{27}$	$\dot{m}_{13} h_{13} + \dot{m}_{26} h_{26} = \dot{m}_{14} h_{14} + \dot{m}_{27} h_{27} + \dot{B}_d$
HRSG	$\dot{m}_4 h_4 + \dot{m}_{27} h_{27} = \dot{m}_5 h_5 + \dot{m}_{28} h_{28}$	$\dot{m}_4 h_4 + \dot{m}_{27} h_{27} = \dot{m}_5 h_5 + \dot{m}_{28} h_{28} + \dot{B}_d$
HX	$\dot{m}_6 h_6 + \dot{m}_8 h_8 = \dot{m}_7 h_7 + \dot{m}_9 h_9$	$\dot{m}_6 h_6 + \dot{m}_8 h_8 = \dot{m}_7 h_7 + \dot{m}_9 h_9 + \dot{B}_d$
INV	$\dot{W}_{dc} = \dot{Q}_{INV} + \dot{W}_{ac}$	$\dot{W}_{dc} = \dot{Q}_{INV} + \dot{W}_{ac} + \dot{B}_d$
G	$\dot{W}_{hf} = \dot{Q}_G + \dot{W}_{lf}$	$\dot{W}_{hf} = \dot{Q}_G + \dot{W}_{lf} + \dot{B}_d$

In Section 3, the equations used to carry out the thermal, exergetic and thermoeconomic analyses are presented, as well as some complementary data taken for the study.

3. Zero-dimensional model

3.1. Thermodynamic analysis

The sizing of the auxiliary components shown in Fig. 1 and Fig. 2 is carried out by using the principle of energy conservation, stated in the first law of thermodynamics. Thus, the energy balances are performed in every component using first-law thermodynamics for control volumes in steady state condition as indicated in Eq. (1). The signs for power and heat transfer rates are considered in accordance with [22].

$$\dot{Q}_{CV} - \dot{W}_{CV} = \sum_{out} \dot{m}_i h_i - \sum_{in} \dot{m}_i h_i \tag{1}$$

In the condition where the fluid exists as a mixture, enthalpy is evaluated in terms of the mass fraction of each compound, x_i, as:

$$h = \sum_{i=1}^{j} x_i h_i \tag{2}$$

As regards reacting systems, like the reformer or the fuel cell stack, the enthalpy h_i per component is evaluated at the corresponding reaction temperature and pressure in terms of the standard enthalpy of formation and the difference in the sensible enthalpy change due to the temperature and pressure change as [23]:

$$h_{i,T,P} = \Delta h^0_{f,298,i} + \left(h_{T,P,i} - h^0_{298,i}\right) \tag{3}$$

The equations of the energy balance for each component are presented in Table 3. Below, other complementary equations required for the design of the components and to perform the energy balance of the system are presented.

3.1.1. Heat exchanger

Heat exchangers are sized according to the number of transfer units

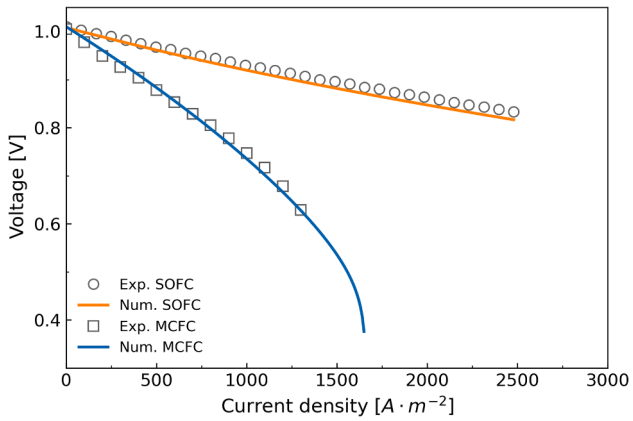

Fig. 4. Electrochemical validation for MCFC and SOFC single cell models operating at 650 °C [25,26].

(NTU) and ε parameters according to the *NTU- ε* method [24]. The NTU is defined as the ratio of the overall heat transfer coefficient to the minimum heat capacity rate.

$$NTU = \frac{UA}{C_{min}} \tag{4}$$

The effectiveness is defined as the ratio of the actual heat transfer rate to the maximum possible heat transfer rate:

$$\varepsilon = \frac{\dot{Q}}{\dot{Q}_{max}} \tag{5}$$

The effectiveness depends on the flow arrangement that a heat exchanger has. In this case a counterflow configuration was used whose relation is:

$$\varepsilon = \frac{1 - \exp[-NTU(1 - C_r)]}{1 - C_r[-NTU(1 - C_r)]} \tag{6}$$

Once the effectiveness and minimum heat capacity rate are known, the actual heat transfer rate is determined as:

$$\dot{Q} = \varepsilon C_{min}(T_{h,i} - T_{c,i}) \tag{7}$$

3.1.2. Heat recovery steam generator

The HRSG is a heat exchanger the function of which is to recover heat content in a hot stream, usually combustion off gases, to produce steam. In this case, the steam produced is mixed with the fuel to produce the stream required in the reformer. The most common HRSG design consists of three sections: economizer, steam generator or evaporator, and steam super-heater, as shown Fig. 3a. Every section consists of pipe arrays in counterflow configuration. The first section is the economizer, the objective of which is to heat the water until saturation temperature. The discharge of the economizer is sent to a deposit drum that contains a mixture of saturated liquid and saturated vapor. The saturated liquid is extracted from the drum in the evaporator where the phase change occurs to obtain saturated vapor. Finally, the saturated vapor flows to the super-heater where it absorbs energy until the desired conditions are reached. A diagram of the temperature versus heat transfer in the HRSG is shown in Fig. 3b indicating the different states of water through it. In order to analyze the HRSG it is necessary to perform an energy balance in every component using Eq. (1).

3.1.3. Fuel cell stack

The two systems studied consist of a MCFC and a SOFC power plants with a nominal capacity of 500kW$_{dc}$ each, as in Fig. 1 and Fig. 2 respectively. In both cases the operating pressure of the stack is 350 kPa and the temperature is analyzed at 600 °C and 650 °C. Accordingly, the operating voltage of the stack is calculated subtracting the ohmic, activation and concentration overpotentials from the Nernst voltage as:

$$V = V_{Nernst} - V_{act} - V_{ohm} - V_{conc} \tag{8}$$

The open-circuit voltage, or Nernst potential, is calculated using Eq. (9)

$$V_{Nernst} = E^0 - \frac{RT}{nF}\ln\left(\frac{\prod_P P_i^k}{\prod_R P_i^j}\right) \tag{9}$$

where E^0 represents the reversible open circuit voltage, p_i is the partial pressure of the i^{th} component of the products, P, or reactants, R, involved in the electrochemical reaction; the exponents k and j indicate the stoichiometric coefficients of the i^{th} component.

The ohmic overpotential accounts for losses due to the flow of electrical current through every component of the cell. The estimation of the ohmic overpotential can be challenging in most cases due to the different nature of the components and their contact resistance once the system is assembled. However, it can be determined experimentally by using the electrochemical impedance spectroscopy (EIS) technique, which is the method used in the present study. The ohmic overpotential has been experimentally estimated by testing single fuel cells, resulting in an ohmic resistance of $R_{ohm} = 1.646\ 1 \times 10^{-2}\ \Omega{\cdot}cm^2$ and $R_{ohm} = 1.976 \times 10^{-1}\ \Omega{\cdot}cm^2$ for MCFC and SOFC at 650 °C, respectively [25,26].

The activation overpotential accounts for the voltage losses required to overcome the activation energy barrier that materials intrinsically display in order to start the electrochemical reaction. It also depends on the temperature and species present in the cell. The model used to estimate the activation overpotentials in the MCFC is presented in [27], with certain parameters recalculated by the authors with experimental data obtained from single cells and reported in [28]. Regarding the SOFC model, this corresponds to the one presented in [29], with certain parameters fitted by the authors with experimental data obtained through SOFC single cell tests.

Finally, the concentration losses account for the effects of mass transport of reactants that have to reach the triple-phase boundary region, where the electrochemical reaction occurs. Fick's law to calculate the concentration overpotential is used in combination with kinetic gas theory to determine the effective binary diffusion coefficient in every electrode. More details are presented in [28].

Table 2 shows the principal dimensions considered for the electrochemical models. It has been assumed that the fuel cell stacks are composed of stack modules. Each MCFC stack module produces 250kW$_{dc}$ operating at 650 °C, as indicated in [19], and the SOFC stack module produces 100kW$_{dc}$ at 850 °C, as indicated in [5].

The electrochemical models have been validated with experimental data obtained through the experimental testing of single cells, as indicated in [25] and [26] for MCFC and SOFC, respectively. The results of the models' validation are shown in Fig. 4, where the single cells were operated at 650 °C.

3.1.4. Reformer

The reforming reaction taking place in the reformer is endothermic. Thus, the heat required to sustain the reaction is provided by the combustion gases coming from the catalytic burner in stream 18, and the rest of the heat is supplied by the fuel cell stack. The heat transfer of the stack is due to the exothermic reaction occurring in the cells and the heat produced by the overpotential losses. It is considered that the reformer and the fuel cell stack are placed together in a container that facilitates the heat transfer process [19]. The energy balance accounting for the heat terms in the reformer is:

$$\dot{Q}_{REF} = \dot{Q}_{FCS,rxn} + I(V_{act} + V_{ohm} + V_{con}) \tag{10}$$

Once the energy balance is carried out in every component and the components have been sized, the next step is to calculate the irreversibilities through an entropy analysis per item of equipment. The design

Table 4
Investment cost for each component.

Component	Cost equation	Reference
FC	$Z_{FC} = 91562\left(\dot{W}_{FC}/455\right)^{0.67}$	[11]
AFC	$Z_{AFC} = 91562\left(\dot{W}_{AFC}/455\right)^{0.67}$	[11]
RC	$Z_{RC} = 91562\left(\dot{W}_{RC}/455\right)^{0.67}$	[11]
P	$Z_P = 705.48\dot{W}_P^{0.71}[1+0.2/(1-\eta_P)]$	[12]
C	$Z_C = \left[71.10\dot{m}_a/(0.9-\eta_C)\right](p_e/p_i)\ln(p_e/p_i)$	[30,33]
T	$Z_T = \left[479.34\dot{m}_g/(0.92-\eta_T)\right]\ln(p_i/p_e)[1+\exp(0.036T_e-54.4)]$	[30,33]
HX	$Z_{HX} = 10000\left[(-0.2478\varepsilon^2-1.238\varepsilon+1.19)/(\varepsilon^2-2.093\varepsilon+1.035)\right]$	[34]
RG	$Z_{RG} = 4122\left[\dot{m}_g(h_i-h_e)/(18\Delta T_{LMTD})\right]^{0.6}$	[30,33]
HRSG	$Z_{HRSG} = 6570\left[\left(\dot{Q}_{ECO}/\Delta T_{LMTD,ECO}\right)^{0.8}+\left(\dot{Q}_{EVA}/\Delta T_{LMTD,EVA}\right)^{0.8}\right]+21276\dot{m}_w+1184.4\dot{m}_g^{1.2}$	[16]
CB	$Z_{CB} = \left[46.08\dot{m}_a/(0.995-P_e/P_i)\right][1+\exp(0.018T_e-26.4)]$	[16,30,33]
ACC	$Z_{ACC} = \left[46.08\dot{m}_a/(0.995-P_e/P_i)\right][1+\exp(0.018T_e-26.4)]$	[16,30,33]
REF	$Z_{REF} = 9.4\times10^6\left(\dot{n}_{CH_4,i}/1390[kmol/h]\right)^{0.6}$	[35]
MCFC	$Z_{MCFC} = 1327\dot{W}_{MCFC}$	[7]
SOFC	$Z_{SOFC} = A_{SOFC}(2.96T_{SOFC}-1907)$	[12]
INV	$Z_{INV} = 10\times10^5\left(\dot{W}_{dc}\right)^{0.7}$	[36,37]
G	$Z_G = 26.18\left(\dot{W}_{ac}\right)^{0.95}$	[38]

parameters of the systems are presented in Table 1.

3.2. Entropy analysis

The first law of thermodynamics is useful to evaluate reversible processes, but actual processes are irreversible. In practice, irreversibilities imply a loss of energy or power which represent an increment in the operational costs. Thus, it is important to perform an entropy analysis in every component in order to identify the critical processes with the highest entropy production. Eq. (11) shows the entropy rate balance for control volumes in steady state [22]:

$$0 = \sum_j \frac{\dot{Q}_j}{T_j} + \sum_i \dot{m}_i s_i - \sum_e \dot{m}_e s_e + \dot{\sigma}_{cv} \tag{11}$$

where $\dot{\sigma}$ is the rate of entropy production.

The properties of real fluids have been taken from the Cantera software. Accordingly, the entropy of any stream at different temperature and pressure can be found in terms of the entropy of the reference state $s^0_{i,T}$

$$s_{i,T,P} = s^0_{i,T} + \left[s_i(T,P) - s_i\left(T,P_{ref}\right)\right] \tag{12}$$

where $s^0_{i,T}$ is evaluated at $T_{ref} = 298.15\ K$ and $P_{ref} = 101.325$ kPa.

3.3. Exergetic analysis

Exergy represents the maximum potential that energy contains to develop work. Thus, this potential is usually measured with respect to the energy a system can convert to work until the thermodynamic equilibrium with the environment is reached. The exergy rate balance for control volumes at steady state with fixed boundaries is stated as [22]:

$$0 = \sum_j \left(1-\frac{T_0}{T_j}\right)\dot{Q}_j - \dot{W}_{CV} + \sum_i \dot{m}_i b_i - \sum_e \dot{m}_e b_e - \dot{B}_d \tag{13}$$

As the work developed by the potential content in exergy could be achieved by physical or chemical means, exergy accounts for both terms that are expressed in Eq. (14) to Eq. (16).

$$b = b^{ph} + b^{ch} \tag{14}$$

$$b^{ph} = (h-h_0) + T_0(s-s_0) \tag{15}$$

$$\overline{b}^{ch} = \sum_{i=1}^{j} y_i \overline{b}_i^{ch} + \overline{R}T_0 \sum_{i=1}^{j} y_i \ln y_i \tag{16}$$

where y is the mole fraction of the i^{th} compound in a flow stream. Table 3 shows the energy and exergy balance equations for every component.

3.4. Economic analysis

In this section, the main assumptions for the estimation of the TCI are presented for each configuration, as well as the LCOE that allows for a better techno-economic comparison of the two configurations. Since the LCOE is a measure of economic competitiveness of different power generation technologies, this parameter will be used to compare the MCFC and SOFC systems allowing to determine the thermo-economic feasibility of each one. In this study, the total revenue requirement method is used to determine the LCOE [30,31].

The equipment costs are estimated by using the cost equation available in the literature for every component, taking into account the operative and design parameters. Table 4 shows the investment cost for each component, including the inverter that converts the direct current provided by the fuel cell stack to alternating current, as well as the electrical generator that converts the high-frequency current produced

Table 5
Detailed information and assumptions of the total capital investment cost estimation [7,30].

Concept	Reference cost
Purchased equipment installation	33 % of PEC
Piping	35 % of PEC
Control and instrumentation	12 % of PEC
Electrical equipment and materials	13 % of PEC
Land cost factor	5 % of PEC
Civil, structural, and architectural factor	30 % of PEC
Service facilities	35 % of PEC
Engineering and supervision	8 % of TDC
Construction cost and contractor's profit	15 % of TDC
Contingency	18.45 % of TDC
Fixed operating and maintenance (O&M)	6.8 % of FCI
Variable operation and maintenance O&M	6.1 % of Fixed O&M

Table 6
Assumptions and parameters for the economic analysis [5,30].

Parameter	Value
Annual inflation rate (%)	2.0
Nominal escalation rate of all services and goods except fuel (%)	2.0
Fuel escalation rate (%)	2.5
Construction period (year) (Jan. 2023–Dec. 2024)	2
Start of commercial operation	01–2025
Economic lifetime for all components except SOFC/MCFC stack (years)	20
Economic lifetime for SOFC/MCFC stack (years)	5
Tax-related plant lifetime (years)	15
Plan for financing	
Common equity	
Fraction (%)	35
Required annual return (%)	8
Preferred stock	
Fraction (%)	15
Required annual return (%)	8
Debt	
Fraction (%)	50
Required annual return (%)	6
Resulting average annual return on investment (%)	7
Income tax rate for company (%)	30
Insurance rate and other taxes rate (%) [7]	5.5
Average annual capacity factor (%)	85
Labor for operating and maintenance (persons)	5
Average labor cost ($/h)	30
Fixed O&M cost (% of PFI) [7]	6.8
Variable O&M cost (% of Fixed O&M) [7]	6.1
Unit cost of fuel (natural gas) ($/GJ-lHV)	15.1
Unit cost of fuel (water) ($/$m^3$) [40]	1.568
Allocation of plant-facilities investment (%)	
Jan. 2023–Dec. 2023	40
Jan. 2024–Dec. 2024	60

by the micro gas turbine into low-frequency current.

In addition to the PEC, more concepts should be considered to carry out the economic analysis, including equipment installation, piping, instrumentation and control, land, service facilities, among others as listed in Table 5. Moreover, Table 5 shows the costs assumptions in terms of the PEC and total direct cost [7,30]. The economic lifetime for all components, except for the fuel cell stacks, is taken as 20 years. The economic lifetime for the SOFC and MCFC stack is considered to be 5 years [5,32]. Thus, during the lifetime of the whole system, a total of 4 replacements, including the initial one, of the fuel cell stacks needs to be done, except for their auxiliaries that remain unchanged.

Table 6 shows additional parameters and assumptions taken for the economic analysis. In the case of fuel cost, also the cost of water is considered, due to the importance of this resource globally. The International Energy Agency (IEA) reports that water and energy will increase their interdependence in the coming years with effects in water availability and reflected in its cost [39]. Once the total capital investment has been determined by considering all the assumptions here presented, the annual total revenue requirement (TRR) is calculated. The TRR represents the amount of money that needs to be obtained in a given year through the sale of all the products in order to compensate the system operation in the same year. It is integrated with two terms: the carrying charges and the expenses [31].

The series of annual costs associated with carrying charges, CC_j, and expenses including fuel cost and operation and maintenance, FF_j and OMC_j, for the j^{th} year of plant operation is not uniform. Thus, a levelized value TRR_L for the total annual revenue requirement is computed by applying a discounting factor and a capital-recovery factor, CRF [30,31]:

$$TRR_L = CRF \sum_{1}^{n} \frac{TRR_j}{\left(1 + i_{eff}\right)^j} \tag{17}$$

where TTR_L is the total revenue requirement in the j^{th} year of the plant operation, i_{eff} is the average annual effective discount rate, and n denotes the plant economic life in years. It is assumed that each money transaction occurs at the end of each year. Thus, the capital-recovery factor (CRF) is expressed as:

$$CRF = \frac{i_{eff}\left(1 + i_{eff}\right)^n}{\left(1 + i_{eff}\right)^n - 1} \tag{18}$$

Once the total revenue requirement is estimated it is possible to obtain the cost of the main product (MPUC). In this study the electricity is the main product. Thus, the cost of electricity (LCOE) is determined by subtracting, in case these are present, the annual total value of by-products (BPV), from the TRR and dividing the result by the main-product quantity (MPQ) as:

$$MPUC = \frac{TRR - BPV}{MPQ} \tag{19}$$

As electricity is the main product and considering it is the only product that can be obtained with this configuration, it is assumed that $LCOE = MPUC$.

The analyses have been performed by solving all the presented equations using Python programming. As for the properties of the substances, they were assumed as real fluids by taking their properties data from the Cantera libraries.

4. Results and discussion

The analyses are carried out in the following order: a) the energy analysis by using first-law thermodynamics to size the devices and determine the operating conditions, b) the entropy analysis using second-law thermodynamics to determine the irreversibilities in each component, c) the exergy analysis by using both first- and second-law thermodynamics to estimate the availability of energy and verify the design of operating conditions, and d) the economic analysis to calculate the LCOE based on the operating conditions.

The pressure, temperature and mass flow rate of fuel in stream 1 of the fuel cell stack are maintained constant. Nevertheless, due to the different energy demands the fuel in stream 23 is calculated in order to fit the design conditions shown in Table 1 and to obtain the 500kW$_{dc}$ delivered by the fuel cell stack.

4.1. Molten carbonate fuel cell system

The first system analyzed is the MCFC/MGT plant, whose configuration is as shown in Fig. 1. The component that provides the main power in the system is the MCFC stack, producing 500kW$_{dc}$. The stack pressure is 350 kPa, and the cell temperature was set at 600 °C and 650 °C. Table 12 and Table 13 show the obtained temperature, pressure, mass flow rate, enthalpy, and composition for every stream at 600 °C and 650 °C, respectively. The water from stream 3 is taken at environment conditions and heated to superheated steam, stream 5, in the HRSG using the remaining heat content from the combustion gases. The fuel

Table 7
Equipment thermal analysis for the MCFC/MGT system.

	600 °C			650 °C		
	η_I[%]	$\dot{W}$[kW]	$\dot{Q}$[kW]	η_I[%]	$\dot{W}$[kW]	$\dot{Q}$[kW]
MCFC	94.12	500.000	−70.201	94.23	500.00	−55.720
T	85.70	333.615	0	85.70	378.056	0
C	79.50	−196.454	0	79.50	−233.434	0
RC	60.00	−28.974	0	60.00	−28.753	0
FC	80.00	−5.854	0	80.00	−5.854	0
AFC	80.00	−0.689	0	80.00	−0.903	0
P	80.00	−0.040	0	80.00	−0.040	0
REF	63.98	0	287.799	56.07	0	299.074
CB	97.00	0	−162.309	97.00	0	−133.541
ACC	97.00	0	−34.370	97.00	0	−28.943
RG	85.74	0	0	98.20	0	0
HRSG	83.38	0	0	88.65	0	0
HX	33.56	0	0	21.07	0	0
G	79.34	0	−28.336	79.34	0	−29.877
INV	94.20	0	−29.000	94.20	0	−29.000

and steam are mixed and heated with the reformed gases in the heat exchanger before entering the reformer. In the latter, the fuel reacts with the steam at high temperatures forming hydrogen through the steam methane reforming and the water-shift reactions, the main reactions involved in hydrogen production. The reformed gas has a molar fraction with a high content of hydrogen, around 50 %; the rest is water vapor, carbon monoxide, carbon dioxide and methane, as shown in Table 12 and Table 13. The reformed gas is supplied to the fuel electrode in the fuel cell stack. The air required in the fuel cell stack is compressed using the compressor of the microturbine. Since the air at the temperature leaving the compressor is not that required by the fuel cell stack, the air is heated again in the regenerator, stream 14, and subsequently mixed with the combustion gases, stream 20. The recirculation of the combustion gases in the MCFC/MGT system is required to maintain the CO_2 concentration in the oxygen electrode and ensure the operation of the cell.

The fuel supplied to the fuel cell stack is not completely consumed in order to avoid damage to the system. The fuel utilization in the fuel electrode at 600 °C and 650 °C is 69.26 % and 65.50 %, respectively. The fuel utilization represents the amount of hydrogen oxidized, methane reformed, and carbon monoxide reacting in the water–gas shift reaction; all these reactions occur in the fuel electrode. At 650 °C the fuel utilization is lower than at 600 °C because at higher temperatures the overpotentials are lower [41], implying less electrical losses and consequently, a lower amount of fuel is required to achieve the 500kW$_{dc}$ in the fuel cell stack.

As stream 10, leaving the fuel electrode, still contains some fuel, it is sent to a catalytic burner to get completely consumed. Stream 16 is the oxidant leaving the fuel cell stack, still rich in oxygen and having a high energy content for use in subsequent processes. Stream 16 is split in two; almost two thirds are sent to the catalytic burner to oxidize the fuel present in stream 10. The combustion gases from the catalytic burner are directed to the reformer. The remnant of stream 16 is directed to the auxiliary combustion chamber and depending on the energy content of the hot gases, it will be determined if extra fuel is added to meet the energetic conditions required in the turbine, regenerator, and the HRSG. Thus, the energy content from stream 25 should be enough to produce power in the turbine to drive the compressor and some extra power. Furthermore, the hot gases from stream 26 should heat up the air to the conditions required by stream 14. Finally, the hot gases leaving the regenerator, stream 27, should heat the water to produce steam and achieve the conditions of stream 5.

The electricity produced by the fuel cell stack and microturbine do not have the characteristics required for integration with the grid. The inverter in the fuel cell stack converts the power produced from direct current into alternating current, just as the generator in the microturbine converts the high-frequency current into low-frequency current, usually, 50 Hz or 60 Hz.

Table 7 shows the efficiency by first-law thermodynamics, i.e. the power and heat transfer rate per piece of equipment in the MCFC/MGT system, at 600 °C and 650 °C. The signs for power and heat transfer rate are considered in accordance with [22], where a positive sign for the power indicates that component generates power, while a negative sign means that power is required by the device. The opposite is assumed for the heat transfer rate, i.e. a positive sign indicates that heat is required by the equipment and the negative sign that heat is produced by the system.

The net power obtained can be determined by adding all the terms of the corresponding column and subtracting the heat losses of the generator and the inverter. At 600 °C and 650 °C, the net power is 544.268 kW and 550.195 kW, respectively. As regarding the efficiency of the components by the first law, the MCFC stack shows an efficiency slightly greater at 650 °C than that at 600 °C because at higher temperatures the overpotentials decrease. Although more power is being produced at 650 °C, due to the higher energy content in the exhaust gases, it is also required to add more fuel to achieve it, as observed from Table 12 and Table 13. Thus, the MCFC/MGT system has a global efficiency by first-law thermodynamics of 46.37 % and 45.39 % at 600 °C and 650 °C, respectively. This result indicates that the system has a slightly better performance at lower temperatures, and this is because at lower temperatures the system consumes less fuel to satisfy the energy requirements in the MCFC/MGT system. The efficiencies are in accordance with reported values of 56.2 % for the conditions analyzed at 600 °C [6] and of 42.89 % at 650 °C [3]. The difference in efficiency compared to [6] is attributed to differences in the electrochemical model used. In the current study, the cell reflects a lower performance compared to other electrochemical models available in literature as

Table 8
Equipment exergy analysis for the MCFC/MGT system.

	600 °C				650 °C			
	$\dot{B}_q$[kW]	$\dot{W}_e$[kW]	$\dot{B}_d$[kW]	η_{II}[%]	$\dot{B}_q$[kW]	$\dot{W}_e$[kW]	$\dot{B}_d$[kW]	η_{II}[%]
MCFC	−47.49	500.00	142.50	72.46	−38.60	500.00	125.19	75.32
T	0	333.61	22.09	93.79	0	378.06	23.78	94.08
C	0	−196.45	16.26	91.72	0	−233.43	19.32	91.72
RC	0	−28.97	3.61	87.56	0	−28.75	3.39	88.22
FC	0	−5.85	0.85	85.52	0	−5.85	0.85	85.52
AFC	0	−0.69	0.10	85.52	0	−0.90	0.13	85.52
P	0	−0.04	0.01	80.00	0	−0.04	0.01	80.00
REF	194.20	0	65.70	88.65	129.73	0	31.57	88.25
CB	−113.27	0	163.83	97.13	−95.81	0	171.79	98.67
ACC	−23.90	0	17.13	94.45	−20.42	0	44.64	92.85
RG	0	0	27.49	84.06	0	0	38.30	85.90
HRSG	0	0	28.26	69.79	0	0	25.99	71.53
HX	0	0	55.87	65.46	0	0	8.57	58.76

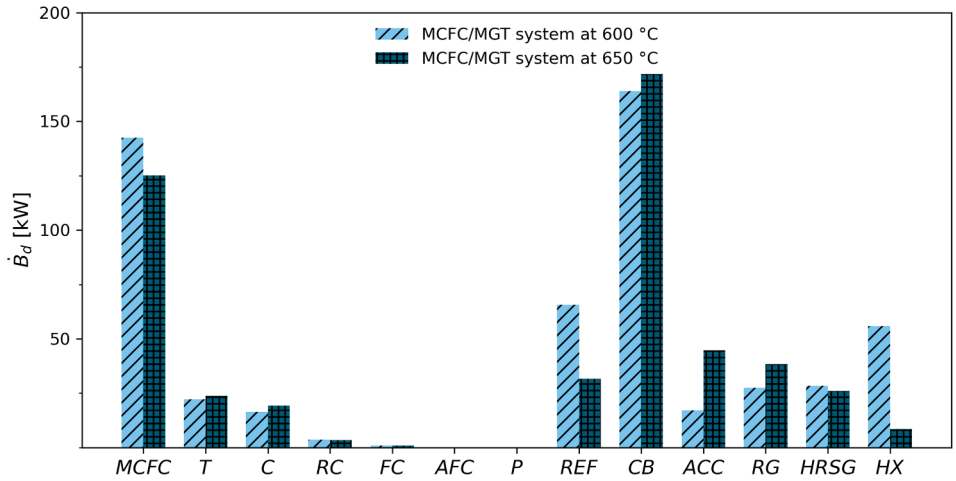

Fig. 5. Comparison of the exergy destruction per piece of equipment in the MCFC/MGT system.

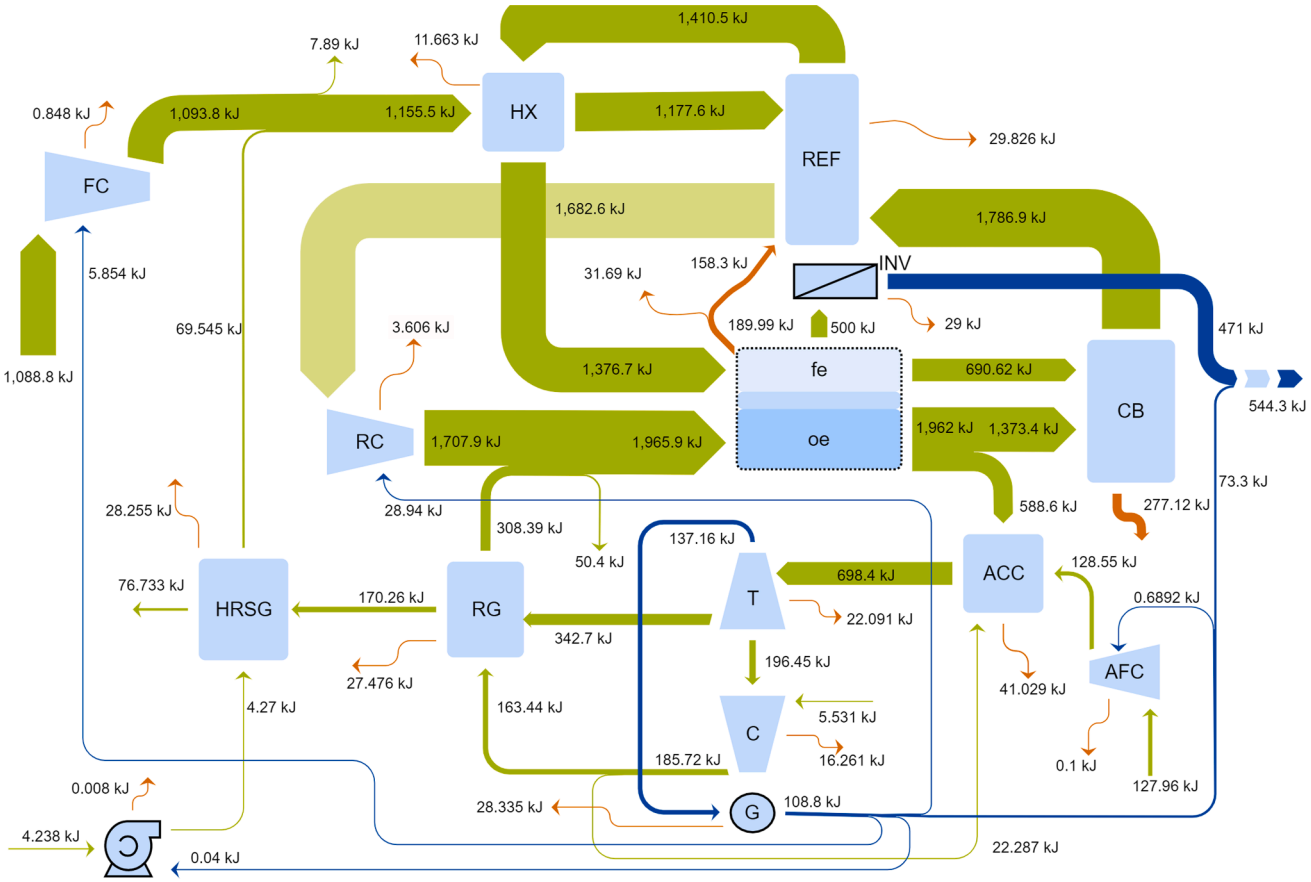

Fig. 6. Sankey diagram of the exergy flows in one second in the MCFC/GT system at 600 °C. The main results are $\dot{m}_1 = 0.021 kg/s$, $\dot{m}_{23} = 0.0025 kg/s$, $\dot{W} = 544.3 kW$, $\eta_I = 46.37\%$, $\eta_{II} = 44.37\%$, and $LCOE = 0.875 \$/kWh$.

shown in [42] being reflected in a lower performance of the system.

Since the analyses carried out by the first law of thermodynamics do not take into account the irreversibilities of the processes, an exergetic analysis is carried out in order to acquire a better understanding of the system. Table 8 shows the exergy results per component at 600 °C and 650 °C for the MCFC/MGT system as well as the second-law efficiency and exergy associated to power and heat transfer rate.

The thermal efficiency of the MCFC stack by the second law of thermodynamics is lower than the one calculated by the first law: the difference is about 20 % lower at both analyzed temperatures. The opposite happens in the reformer, which shows an improvement in the efficiency when it is calculated using second-law thermodynamics. The difference between the 1st and 2nd law efficiency is because the first law does not take into account the use of heat by entropy generation. Fig. 5 shows a comparison of the exergy destruction per component. Since the exergy destruction is a measure of the irreversibilities present in the system, the components with higher irreversibilities are the catalytic burner, the MCFC stack, and the reformer. In these components the irreversibilities tend to increase because of the chemical reactions that take place there. The CB has the highest exergy destruction, occuring

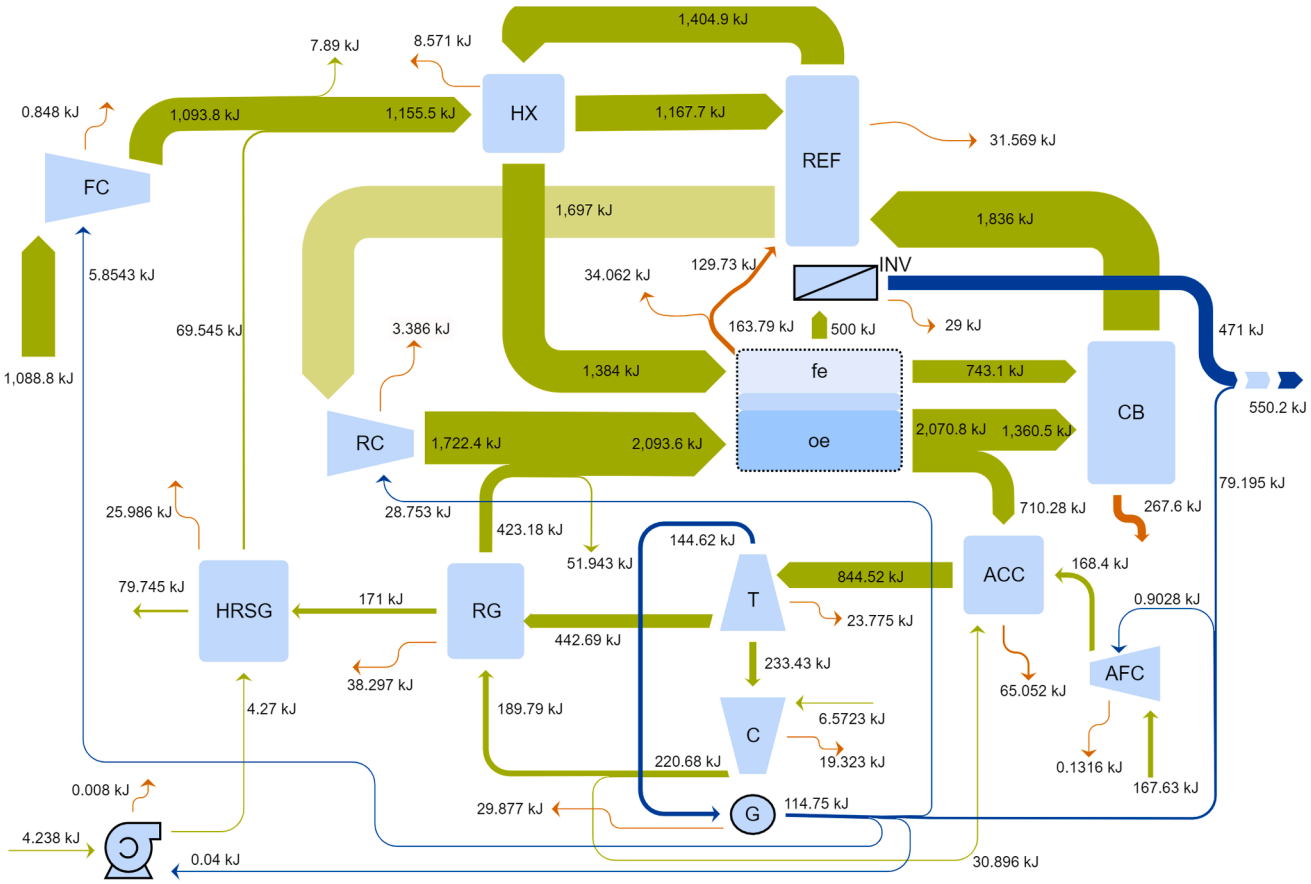

Fig. 7. Sankey diagram of the exergy flows in one second in the MCFC/MGT system at 650 °C. The main results are $\dot{m}_1 = 0.021 kg/s$, $\dot{m}_{23} = 0.0032 kg/s$, $\dot{W} = 550.2 kW$, $\eta_I = 45.39\%$, $\eta_{II} = 44.42\%$, and $LCOE = 0.897 \$/kWh$.

when the MCFC system operates at 650 °C. At higher temperatures the CB demands more fuel to maintain the design conditions in the regenerator and HRSG to heat the air and the water, respectively. El-Emam [3] indicates that the CB presents the highest exergy destruction followed by the ACC, HRSG, reformer and fuel cell.

The exergy flows are represented in the Sankey diagrams of Fig. 6 and Fig. 7 for the MCFC/MGT system at 600 °C and 650 °C, respectively. The Sankey diagrams for the MCFC/MGT system are built with Table 8, Table 16, and Table 17. The exergy interaction between all the components in the MCFC/MGT system is represented in the Sankey diagrams as well. It can be observed that the mixing process also produces some irreversibilities, e.g. the mixture of steam, stream 5, with methane, stream 2, before entering the heat exchanger.

The heat losses plus the exergy destruction or irreversibilities are accounted for in the general losses represented by the red lines drawn in the Sankey diagrams. The exergy destruction is generally manifested as heat losses. The MCFC stack and the reformer are mounted in the same compartment to take advantage of the exothermic nature of the oxidation reaction in the fuel electrode of the stack to sustain the endothermic reaction in the reformer. Such an arrangement helps to decrease the temperature in the fuel cell stack because the heat produced by the stack can be absorbed by the reformer.

It can be observed from the Sankey diagrams of Fig. 6 and Fig. 7 that more exergy losses are present in the fuel cell stack at 600 °C than at 650 °C because at higher temperatures the overpotentials decrease, helping to produce also less exergy destruction. Although less heat is available to be absorbed by the reformer at 650 °C, it requires a lower heat transfer rate from the MCFC stack because at higher temperatures the exergy in stream 18 increases, supplying more energy from the hot gases. Furthermore, some exergy streams are almost constant because the STC ratio is fixed, including the fuel compressor exit, stream 2, the pump exit, stream 4, and the HRSG cold side, stream 5. Moreover, the temperature at which the fuel is being reformed is kept almost constant because the amount of fuel does not change.

The thermal efficiency by second-law thermodynamics can also be calculated from Fig. 6 and Fig. 7. The efficiency is determined by dividing the product, in this case the electricity, over the exergy inputs that involves the fuel of streams 1 and 23, the water exergy of stream 3 and the air exergy in stream 11. Thus, the thermal efficiency by the second law for the MCFC system is 44.37 % and 43.42 % at 600 °C and 650 °C, respectively, which is in accordance with reported values [3,6]. Accordingly, both the first- and second-law thermal efficiencies are improved when the fuel cell stack operates at lower temperatures, because less fuel reacts to maintain lower temperatures. The second law efficiencies show a slight decrease compared to those obtained by the first law, i.e. the 2nd law efficiencies are slightly lower than the 1st law efficiencies. This is because the exergetic analysis considers the irreversibilities present in every component, as clearly observed in the arrangement reformer-fuel cell stack the interactions of exergy, Fig. 6 and Fig. 7.

4.2. Solid Oxide fuel cell system

The SOFC/MGT system configuration analyzed in this section is shown in Fig. 2. The nomenclature in the streams and components is the same as that used in the MCFC/MGT system. Nevertheless, the SOFC/MGT system does not include a re-compressor for the gases leaving the reformer, because in this case the hot gases are sent directly to the auxiliary combustion chamber independently of the pressure drop. The other difference compared to the MCFC/MGT system is in the stream

Table 9
Equipment thermal analysis for the SOFC/MGT system.

	600 °C			650 °C		
	η_I[%]	$\dot{W}$[kW]	$\dot{Q}$[kW]	η_I[%]	$\dot{W}$[kW]	$\dot{Q}$[kW]
SOFC	93.89	500.000	−158.255	93.90	500.000	−152.732
T	85.70	325.293	0	85.70	251.545	0
C	79.50	−191.370	0	79.50	−130.922	0
RC	0	0	0	0	0	0
FC	80.00	−5.854	0	80.00	−5.854	0
AFC	80.00	−0.199	0	80.00	0	0
P	80.00	−0.040	0	80.00	−0.040	0
REF	82.50	0	284.039	72.62	0	299.048
CB	97.00	0	−29.795	97.00	0	−31.810
ACC	97.00	0	−32.490	100.00	0	0
RG	88.13	0	0	84.67	0	0
HRSG	82.97	0	0	77.57	0	0
HX	31.67	0	0	21.06	0	0
G	79.34	0	−27.667	79.34	0	−24.919
INV	94.20	0	−29.000	94.20	0	−29.000

split after the oxygen electrode, where a percentage of the air leaving the oxygen electrode is directed to the catalytic burner to provide the oxygen required to oxidize the fuel content in stream 10 leaving the fuel electrode; the rest of the air is recirculated to the oxygen electrode. Due to the reactions that occur in the SOFC stack, the oxygen content decreases in the cathode, from stream 15 to stream 16, as observed from Table 14 and Table 15 at 600 °C and 650 °C, respectively. The reduction in the mole fraction of the oxygen is from 16.57 % to 15.44 %, when the temperature is 600 °C, and from 14.85 % to 13.71 % when the temperature is 650 °C; in both cases the diminution is almost the same. Thus, the fresh air supplied by the compressor, stream 14, helps to compensate the consumption of oxygen in the fuel cell stack when is mixed with the air leaving the oxygen electrode, stream 21. The operation of the other components is similar to those in the MCFC/MGT system, which have been previously described. The power supplied by the SOFC stack is also 500kW$_{dc}$, the operating pressure is 350 kPa, and the cell temperature was set to 600 °C and 650 °C. The air-to-fuel ratio was kept constant as $\dot{m}_{15}/\dot{m}_9 = 39.2054$, as well as the steam-to-carbon ratio, $\dot{m}_4/\dot{m}_1 = 4.04$. Table 14 and Table 15 show the temperature, pressure, mass flow rate, enthalpy, and composition for each stream at 600 °C and 650 °C, respectively.

Table 9 shows the first-law efficiency, power, and heat transfer rate per component in the SOFC/MGT system at 600 °C and 650 °C. The efficiency of the SOFC stack is almost the same at both temperatures and slightly lower compared to the efficiency of the MCFC stack at the same temperatures, where the higher difference between the SOFC and MCFC stack first-law efficiency is only 0.33 % at 650 °C. The overall first-law efficiency of the SOFC/MGT system is 52.59 % and 53.39 % at 600 °C and 650 °C, respectively. These efficiency values are in accordance with [43] where data for a hybrid SOFC system at this temperature range is presented. In this sense, it resulted to be a more efficient configuration than using an MCFC stack. The difference in efficiency is about 7–8 %. In this study both fuel cell stacks, MCFC and SOFC, produce the same power at the two analyzed temperatures, 500kW$_{dc}$, by adjusting the current density. The net power obtained with the SOFC/MGT system is 571.162 kW at 600 °C and 560.810 kW at 650 °C. The power obtained with the SOFC system at 600 °C is higher than the one obtained at

Table 10
Equipment exergy analysis for the SOFC/MGT system.

	600 °C				650 °C			
	$\dot{B}_q$[kW]	$\dot{W}_e$[kW]	$\dot{B}_d$[kW]	η_{II}[%]	$\dot{B}_q$[kW]	$\dot{W}_e$[kW]	$\dot{B}_d$[kW]	η_{II}[%]
SOFC	−107.06	500.00	174.09	64.01	−105.95	500.00	166.45	64.73
T	0	325.29	21.55	93.79	0	251.54	15.53	94.18
C	0	−191.37	15.84	91.72	0	−130.92	10.84	91.72
RC	0	0	0	0	0	0	0	0
FC	0	−5.85	0.85	85.52	0	−5.85	0.85	85.52
AFC	0	−0.20	0.03	85.52	0	0	0	0
P	0	−0.04	0.01	80.00	0	−0.04	0.01	80.00
REF	197.23	0	29.93	88.46	209.67	0	52.90	81.76
CB	−21.95	0	159.95	97.21	−24.08	0	147.71	94.86
ACC	22.60	0	48.12	96.38	0	0	17.77	33.55
RG	0	0	21.62	86.84	0	0	23.74	82.05
HRSG	0	0	29.02	69.22	0	0	33.41	66.15
HX	0	0	11.02	64.53	0	0	8.57	58.76

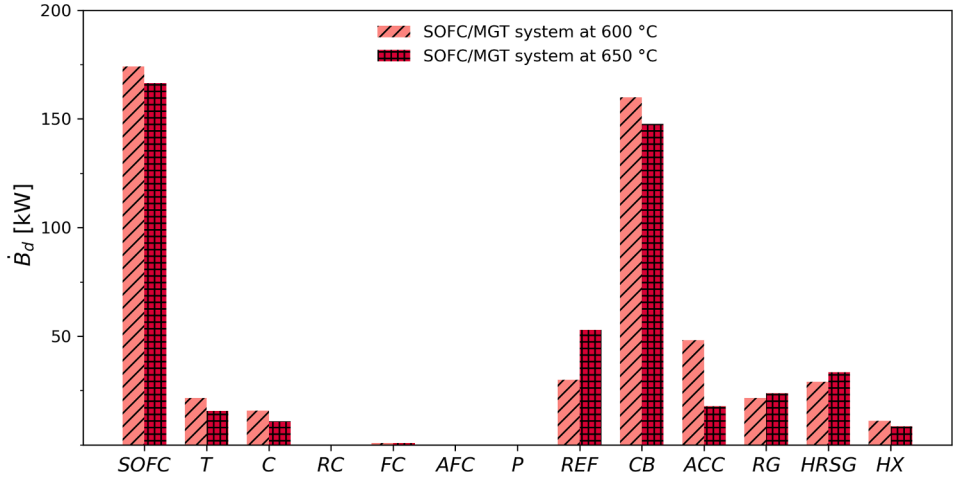

Fig. 8. Exergy destruction per piece of equipment in the SOFC/MGT system.

Table 11
MCFC/GT and SOFC/GT system comparison.

	600 °C		650 °C	
	MCFC	SOFC	MCFC	SOFC
Stack 1st law efficiency, %	94.12	93.89	94.23	93.9
System 1st law efficiency, %	46.37	52.59	45.39	53.39
Stack 2st law efficiency, %	72.46	64.01	75.32	64.01
System 2st law efficiency, %	44.37	50.3	43.42	51.13
PEC of fuel cell stack	$ 663,500.00	$ 135,504.80	$ 663,500.00	$ 103,190.50
PEC of the system	$ 3,489,913.74	$ 1,328,761.01	$ 3,617,099.94	$ 996,721.85
TNCI at the begining	$ 14,832,663.47	$ 5,751,008.48	$ 15,370,453.36	$ 4,353,471.34
LCOE, $/kWh	0.875	0.402	0.897	0.339
CO2 expelled, kg/year	479.39	443.61	495.11	429.02

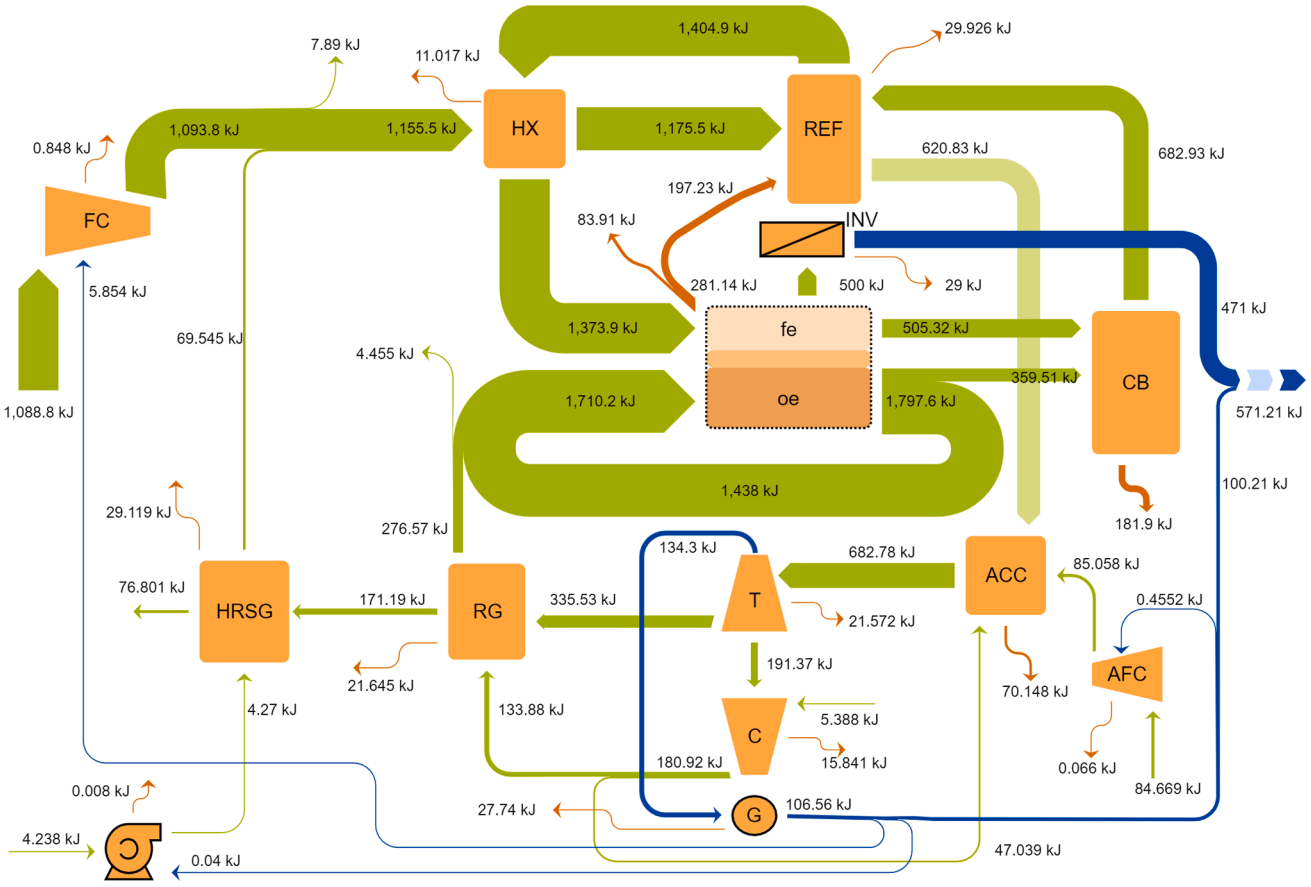

Fig. 9. Sankey diagram of the exergy flow in one second in the SOFC/MGT system at 600 °C. The main results are $\dot{m}_1 = 0.021 kg/s$, $\dot{m}_{23} = 0.0007 kg/s$, $\dot{W} = 571.2 kW$, $\eta_I = 52.59\%$, $\eta_{II} = 50.30\%$, and $LCOE = 0.402 \$/kWh$.

650 °C, but the efficiency is lower, which can be explained because more fuel is required to satisfy the energetic conditions at this temperature. The differences in efficiency are due to the configuration of the auxiliary components that affects the overall efficiency. In the case of the SOFC/MGT system, the efficiency improves compared to the MCFC/MGT system. This is because more power can be obtained from the microturbine due to a reduction in the power required by the compressor to supply less air in stream 14, which mixes with the recirculation gases prior to enter the oxygen electrode.

The results of the exergetic analysis for the SOFC/MGT system are presented in Table 10 where the exergy streams and second-law thermal efficiency are shown, considering the irreversibilities present in every component. The second-law efficiency of the SOFC stack is 64.01 % and 64.73 % at 600 °C and 650 °C, respectively. In both cases the second-law thermal efficiency of the SOFC stack is lower than the efficiency obtained in the MCFC stack by 8.45 % at 600 °C and 10.26 % at 650 °C. Most of the components show an improved efficiency at 600 °C, except for the gas turbine. The components with the higher exergy destruction are the catalytic burner, the SOFC stack, and the reformer, as in the MCFC/MGT system. Fig. 8 shows a comparison of the exergy destruction per equipment in the SOFC/MGT system. The exergy destruction is higher in the SOFC stack than in the MCFC stack due to a lower efficiency of the former. Nevertheless, most of the components show a lower exergy destruction in the SOFC/MGT system than in the MCFC/MGT system, being this latter generally less efficient. Table 11 presents a general comparison of the thermal and exergy comparison of both fuel cell systems.

Table 18 and Table 19 show the exergy flows per stream, while Fig. 9 and Fig. 10 show the interaction of the exergy flows per piece of equipment, including the exergy by power, heat transfer rate and exergy destruction, in accordance with the configuration of the SOFC/MGT system shown in Fig. 2. The second-law thermal efficiency is calculated

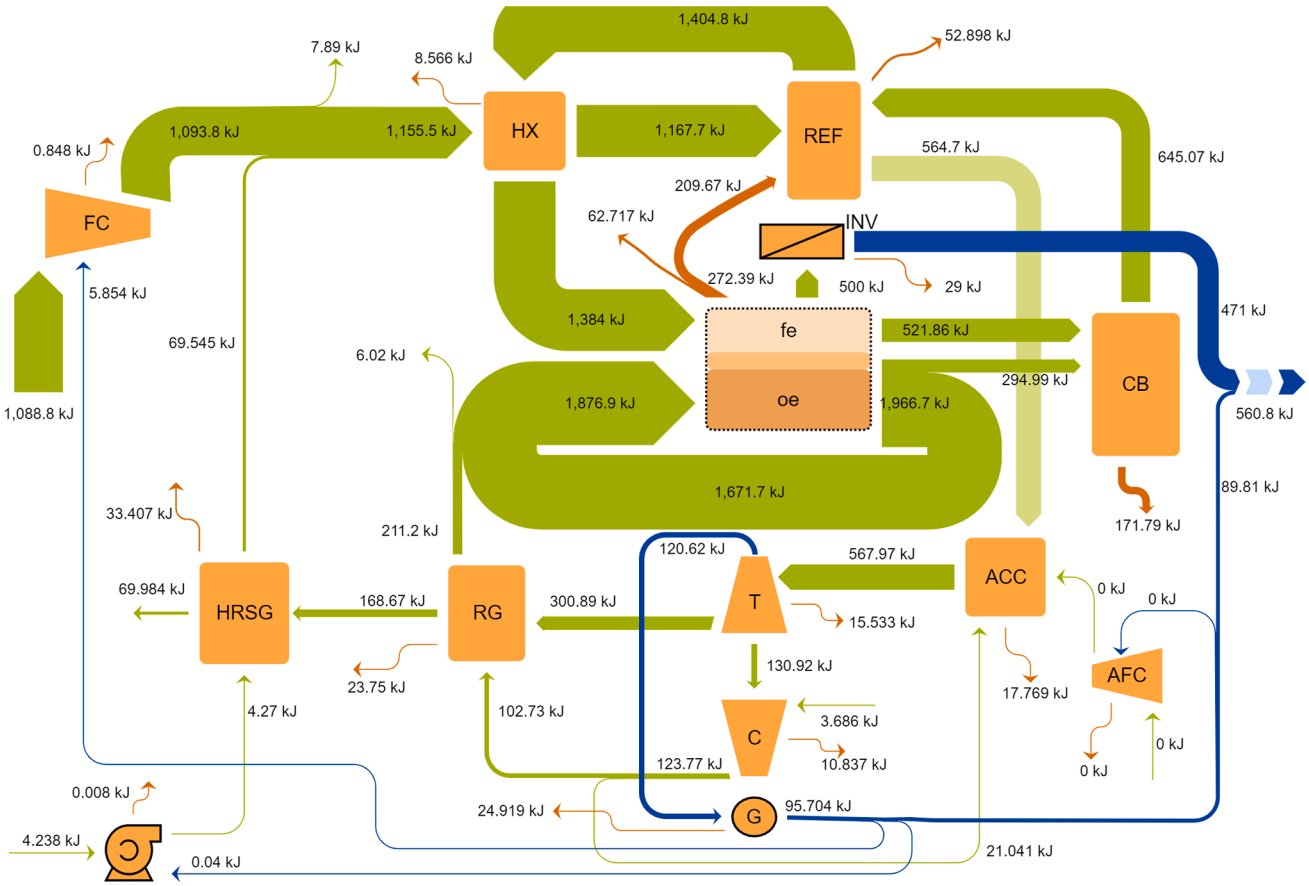

Fig. 10. Sankey diagram of the exergy flow in one second in the SOFC/MGT system at 650 °C. The main results are $\dot{m}_1 = 0.021 kg/s$, $\dot{m}_{23} = 0 kg/s$, $\dot{W} = 560.8 kW$, $\eta_I = 53.39\%$, $\eta_{II} = 51.13\%$, and $LCOE = 0.339 \$/kWh$.

as described in the previous section. Accordingly, for the SOFC/MGT system these are 50.30 % at 600 °C and 51.13 % at 650 °C. In the SOFC system, the efficiency improved when the temperature of the fuel cell stack increased, allowing to save the fuel flow from stream 23, as shown in Fig. 10. The cancellation of fuel in stream 23 was possible thanks to an increase in the air flow recirculation from stream 21, demanding less fresh air from the compressor. A lower amount of fresh air reduces the energy demand in the regenerator. Most of the oxygen and energy required by the fuel cell stack is recirculated at the exit of the cathode, stream 16, to the inlet, stream 15. In the SOFC/MGT system the number of modules was calculated in order to satisfy the energy conditions in the reformer-fuel cell stack pair. The number of modules decreases from 8 to 5 when the temperature increases from 600 °C to 650 °C, increasing the current density and consequently the overpotentials, then achieving the heat transfer rate demanded by the reformer. The reduction in the number of modules agrees with the results presented by [44] indicating that the power provided by the SOFC stack improves with the increase of temperature. This fact allows to decrease the required area of the stack, reflected in the number of modules, to fit a target power that in this case was $500 kW_{dc}$.

4.3. Economic and environmental analysis

In this section some economic and environmental aspects between the two analyzed systems will be covered. Most of the assumptions considered for the economic analysis are presented in Table 4, Table 5, and Table 6. In these, respectively, the investment equations per component, the assumptions for the total capital investment and the parameters for the economic analysis are indicated. It is considered that both systems have an economic lifetime of 20 years, with the exception of the fuel cell stacks that have an economic lifetime of 5 years. Thus, three replacements of the fuel cell stacks should be done in the whole lifetime of the system, representing a purchase of four complete fuel cell stacks. The PEC for the MCFC stack is $663,500.00 at both temperatures because its cost depends only on the desired power [7]. The PEC for the SOFC stack depends on the active area of the cell and the cell temperature, as indicated in Table 4. The number of SOFC stack modules was varied with temperature to maintain the same voltage range, using 8 modules at 600 °C and 5 modules at 650 °C. Thus, the SOFC active area is 200 m^2 at 600 °C and 125 m^2 at 650 °C representing a PEC of $135,504.80 and $103,190.50, respectively [12]. This is about 5 and 6 times cheaper than the cost of the MCFC stack. The PEC of the other components depends on the operating conditions which can be determined with the equations of Table 4 and the design conditions of the systems presented in Table 12, Table 13, Table 14, and Table 15. The total PEC of the MCFC/MGT system is $3,489,913.74 at 600 °C and $3,617,099.94 at 650 °C, resulting in this case being more expensive at higher temperatures because of the robustness required for some components when increasing the temperature. The contrary happens with the total PEC for the SOFC/MGT system, being $1,328,761.01 at 600 °C and $996,721.85 at 650 °C, because of the reduction in the number of SOFC stacks at higher temperatures, as well as the required robustness in some components due to a reduction of the mass flow rate in stream 17. The total net capital investment, TNCI, required in the beginning of the projects is estimated by considering the parameters presented in Table 5 and Table 6 for the economic lifetime of the systems. The TNCI for the MCFC/MGT system is $14,832,663.47 at 600 °C and $15,370,453.36 at 650 °C, while the TNCI for the SOFC/MGT system is $5,751,008.48 at 600 °C and $4,353,471.34 at 650 °C, indicating an almost 3 times lower investment than for the MCFC/MGT system.

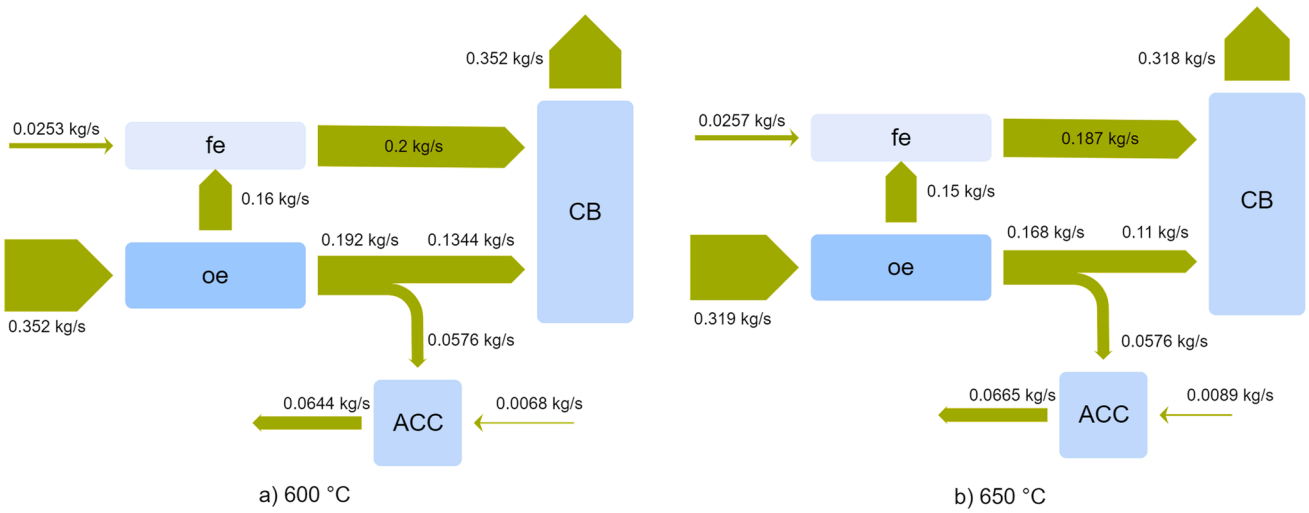

Fig. 11. Sankey diagram of the flow of carbon dioxide in the MCFC/MGT system at: (a) 600 °C and (b) 650 °C.

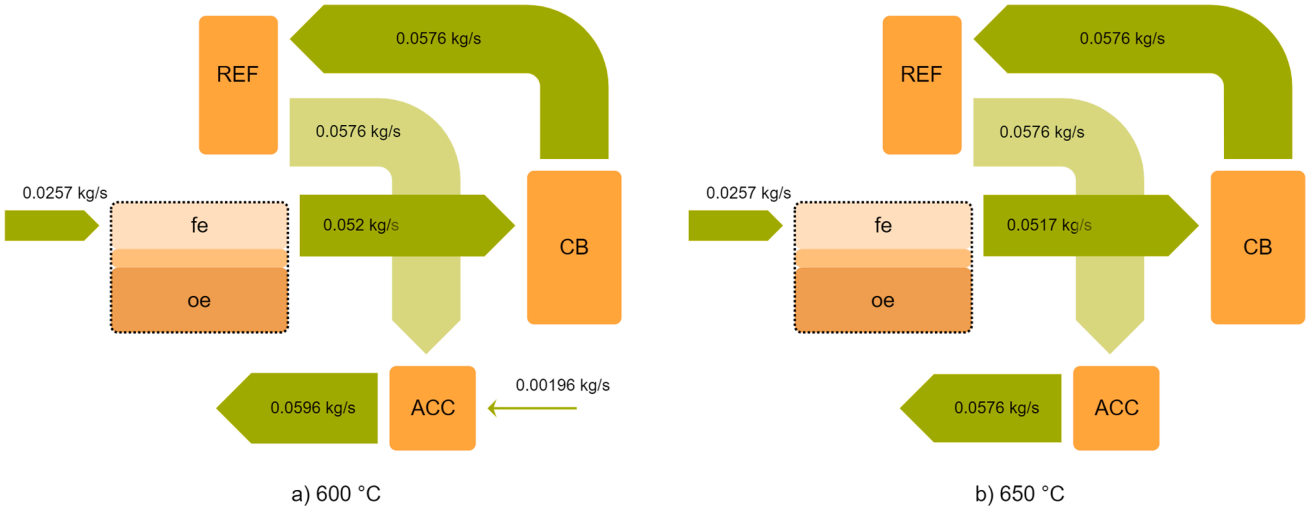

Fig. 12. Sankey diagram of the flow of carbon dioxide in the SOFC/MGT system at: (a) 600 °C and (b) 650 °C.

The total revenue requirement method was used to estimate the LCOE for each system according to [30]. The LCOE is 0.875$/kWh at 600 °C and 0.897$/kWh at 650 °C for the MCFC/MGT system, while for the SOFC/MGT system is 0.402$/kWh at 600 °C and 0.339$/kWh at 650 °C. The costs for the SOFC/MGT system are in accordance with [5] that reports values of 0.320$/kWh at 650 °C and 101.325 kPa. In the case of the MCFC/MGT system it can be compared with the price of the standalone system reported in [7] to be 0.186$/kWh, although there is no clear indication whether the replacements of the stack have been taken in consideration. The cheapest option thus results when the SOFC/MGT system is operated at 650 °C, which is thanks to the reduction in the number of SOFC stacks and the improvement in the efficiency. The LCOE using the MCFC/MGT system doubles the value obtained using the SOFC/MGT system.

According to the TNCI and the LCOE obtained, the MCFC/MGT system seems to be an expensive option to produce electricity, compared to the SOFC/MGT system. Nevertheless, the MCFC stacks have also the characteristic to separate the carbon dioxide present in the cathode to the anode by migration through the carbonate ion. This is a characteristic which is not present in the SOFC stacks. This peculiarity can help to mitigate the high TNCI and to decrease the LCOE by implementing configurations that help to reutilize the carbon dioxide instead of expelling it directly to the environment. For example, in [14] the products of reducing the CO_2 are considered obtaining LCOE between 0.020 and 0.225$/kWh. Fig. 11 shows a Sankey diagram of the carbon dioxide flow in the MCFC stack, the catalytic burner, and the auxiliary combustion chamber at 600 °C and 650 °C. Besides, Fig. 12 shows a Sankey diagram of the carbon dioxide flow in the SOFC stack with its interaction with the catalytic burner, the reformer, and the auxiliary combustion chamber at 600 °C and 650 °C. The amount of carbon dioxide entering the fuel electrode corresponds to the CO_2 replaced in the reformer, while the amount of CO_2 entering the oxygen electrode corresponds to the quantity being recirculated from the catalytic burner. In both stacks, the CO_2 recirculated is 12.5–14 times higher than the CO_2 coming from the reformer.

In the MCFC/MGT configuration the CO_2 required in the oxygen electrode is obtained by recirculating the gases. Nevertheless, there are configurations where the CO_2 is supplied from combustion gases that usually are expelled to the environment [15]. In such a case, the MCFC could help to decrease the CO_2 sent to the atmosphere in the combustion gases, because the oxygen electrode directs some CO_2 to the fuel electrode. In carbon capture applications MCFC can be coupled with traditional power plants decreasing the emission to the atmosphere by approximately 62 % [15]. It can be observed from Fig. 11 that between 45 % and 47 % of the CO_2 passes to the fuel electrode. The CO_2 at the exit of the fuel electrode is mixed with other compounds including water,

Table 12
Thermal results for the MCFC system at 600 °C.

	T[°C]	p[Pa]	$\dot{m}$[kg/s]	h[kg/s]	CO[%]	CO_2[%]	CH_4[%]	H_2[%]	H_2O[%]	N_2[%]	O_2[%]
1	15.00	101 325	0.0210	32.93	0	0	100	0	0	0	0
2	133.20	368 000	0.0210	311.70	0	0	100	0	0	0	0
3	15.00	101 325	0.0848	63.02	0	0	0	0	100	0	0
4	15.03	476 000	0.0848	63.49	0	0	0	0	100	0	0
5	180.00	368 000	0.0848	2 820.51	0	0	0	0	100	0	0
6	169.07	368 000	0.1058	2 322.73	0	0	21.75	0	78.25	0	0
7	369.40	361 000	0.1058	2 775.08	0	0	21.75	0	78.25	0	0
8	756.89	357 000	0.1058	3 276.53	7.97	6.73	0.66	50.83	33.81	0	0
9	600.00	350 000	0.1058	2 824.19	7.97	6.73	0.66	50.83	33.81	0	0
10	635.00	349 000	0.3235	1 797.03	2.67	37.49	0.46	8.73	50.65	0	0
11	15.00	101 325	1.2201	15.48	0	0	0	0	1	78.20	20.80
12	157.76	357 000	1.2201	176.49	0	0	0	0	1	78.20	20.80
13	157.76	357 000	1.0737	176.49	0	0	0	0	1	78.20	20.80
14	425.94	350 000	1.0737	460.18	0	0	0	0	1	78.20	20.80
15	600.00	350 000	4.1495	977.30	0	5.33	0	0	17.11	64.91	12.66
16	635.00	349 000	3.9319	1 041.33	0	3.02	0	0	17.75	67.35	11.88
17	635.00	349 000	2.7523	1 041.33	0	3.02	0	0	17.75	67.35	11.88
18	680.66	347 000	3.0758	1 195.95	0	7.09	0	0	22.45	60.50	9.96
19	644.47	343 000	3.0758	1 148.40	0	7.09	0	0	22.45	60.50	9.96
20	651.66	350 000	3.0758	1 157.82	0	7.09	0	0	22.45	60.50	9.96
21	635.00	349 000	1.1796	1 041.33	0	3.02	0	0	17.75	67.35	11.88
22	157.76	357 000	0.1464	176.49	0	0	0	0	1	78.20	20.80
23	15.00	101 325	0.0025	32.93	0	0	100	0	0	0	0
24	133.38	368 000	0.0025	312.16	0	0	100	0	0	0	0
25	673.01	348 000	1.3284	1 063.46	0	3.01	0	0	16.57	68.28	12.14
26	470.24	108 000	1.3284	812.32	0	3.01	0	0	16.57	68.28	12.14
27	276.17	104 000	1.3284	583.03	0	3.01	0	0	16.57	68.28	12.14
28	121.54	101 325	1.3284	406.96	0	3.01	0	0	16.57	68.28	12.14

Table 13
Thermal results for the MCFC system at 650 °C.

	T[°C]	p[Pa]	$\dot{m}$[kg/s]	h[kg/s]	CO[%]	CO_2[%]	CH_4[%]	H_2[%]	H_2O[%]	N_2[%]	O_2[%]
1	15.00	101 325	0.0210	32.93	0	0	100	0	0	0	0
2	133.20	368 000	0.0210	311.70	0	0	100	0	0	0	0
3	15.00	101 325	0.0848	63.02	0	0	0	0	100	0	0
4	15.03	476 000	0.0848	63.49	0	0	0	0	100	0	0
5	180.00	368 000	0.0848	2 820.51	0	0	0	0	100	0	0
6	169.07	368 000	0.1058	2 322.73	0	0	21.75	0	78.25	0	0
7	291.54	361 000	0.1058	2 596.64	0	0	21.75	0	78.25	0	0
8	744.68	357 000	0.1058	3 240.42	7.68	6.89	0.85	50.58	34.00	0	0
9	650.00	350 000	0.1058	2 966.52	7.68	6.89	0.85	50.58	34.00	0	0
10	679.00	349 000	0.3117	1 903.43	3.43	35.72	0.61	9.30	50.95	0	0
11	15.00	101 325	1.4498	15.48	0	0	0	0	1	78.20	20.80
12	157.76	357 000	1.4498	176.49	0	0	0	0	1	78.20	20.80
13	157.76	357 000	1.2468	176.49	0	0	0	0	1	78.20	20.80
14	503.63	351 000	1.2468	545.43	0	0	0	0	1	78.20	20.80
15	650.00	350 000	4.1495	998.92	0	4.86	0	0	15.17	66.30	13.67
16	679.00	349 000	3.9437	1 052.20	0	2.65	0	0	15.72	68.67	12.96
17	679.00	349 000	2.5910	1 052.20	0	2.65	0	0	15.72	68.67	12.96
18	746.67	347 000	2.9027	1 249.79	0	6.85	0	0	20.99	61.42	10.74
19	696.59	343 000	2.9027	1 183.81	0	6.85	0	0	20.99	61.42	10.74
20	704.14	350 000	2.9027	1 193.71	0	6.85	0	0	20.99	61.42	10.74
21	679.00	349 000	1.3527	1 052.20	0	2.65	0	0	15.72	68.67	12.96
22	157.76	357 000	0.2030	176.49	0	0	0	0	1	78.20	20.80
23	15.00	101 325	0.0032	32.93	0	0	100	0	0	0	0
24	133.38	368 000	0.0032	312.16	0	0	100	0	0	0	0
25	705.00	348 000	1.5589	1 058.95	0	2.67	0	0	14.54	69.61	13.18
26	508.22	117 000	1.5589	816.43	0	2.67	0	0	14.54	69.61	13.18
27	255.92	104 000	1.5589	521.34	0	2.67	0	0	14.54	69.61	13.18
28	122.29	101 325	1.5589	371.29	0	2.67	0	0	14.54	69.61	13.18

carbon monoxide, hydrogen, and methane, where the water and carbon dioxide are the components with the higher mole fraction, as can be observed in Table 12 and Table 13. The fuel in stream 10, which includes methane, hydrogen, and carbon monoxide, is mixed with oxidant in the catalytic burner increasing the temperature of the gases sent to the reformer. Thus, the composition of stream 18 includes only steam and three non-condensable gases: carbon dioxide, oxygen and nitrogen. The CO_2 could be separated from the other gases, although, in this configuration is quite complicated because of the presence of non-condensable gases. Thus, other options should be explored in order to facilitate the separation of the CO_2 from the combustion gases. For example, using only oxygen to oxidize the fuel in stream 10, or eventually separate all the gases and see them as products that can be sold [45]. The oxidant that is not sent to the catalytic burner is directed to the auxiliary combustion chamber, and some fuel is added to achieve the energy conditions required in the upstream components to finally reach the environment. Accordingly, the annual amount of CO_2 expelled to the atmosphere resulted to be 479.39 kg/year and 495.11 kg/year at 600 °C

Table 14
Thermal results for the SOFC system at 600 °C.

	T[°C]	p[Pa]	ṁ[kg/s]	h[kg/s]	CO[%]	CO_2[%]	CH_4[%]	H_2[%]	H_2O[%]	N_2[%]	O_2[%]
1	15.00	101 325	0.0210	32.93	0	0	100	0	0	0	0
2	133.20	368 000	0.0210	311.70	0	0	100	0	0	0	0
3	15.00	101 325	0.0848	63.02	0	0	0	0	100	0	0
4	15.03	476 000	0.0848	63.49	0	0	0	0	100	0	0
5	180.00	368 000	0.0848	2 820.51	0	0	0	0	100	0	0
6	169.07	368 000	0.1058	2 322.73	0	0	21.75	0	78.25	0	0
7	354.07	361 000	0.1058	2 739.52	0	0	21.75	0	78.25	0	0
8	744.82	357 000	0.1058	3 240.81	7.68	6.88	0.85	50.58	34.00	0	0
9	600.00	350 000	0.1058	2 824.03	7.68	6.88	0.85	50.58	34.00	0	0
10	635.00	349 000	0.1679	2 843.20	0.63	13.93	0.85	11.97	72.61	0	0
11	15.00	101 325	1.1886	15.48	0	0	0	0	1	78.20	20.80
12	157.76	357 000	1.1886	176.49	0	0	0	0	1	78.20	20.80
13	157.76	357 000	0.8795	176.49	0	0	0	0	1	78.20	20.80
14	467.13	351 000	0.8795	505.19	0	0	0	0	1	78.20	20.80
15	600.00	350 000	4.1495	656.56	0	0	0	0	1.05	82.38	16.57
16	635.00	349 000	4.0875	697.28	0	0	0	0	1.07	83.49	15.44
17	635.00	349 000	0.8175	697.28	0	0	0	0	1.07	83.49	15.44
18	821.78	347 000	0.9854	1 356.35	0	3.58	0	0	20.85	65.35	10.23
19	758.05	343 000	0.9854	1 271.31	0	3.58	0	0	20.85	65.35	10.23
20	0	0	0	0	0	0	0	0	0	0	0
21	635.00	349 000	3.2700	697.28	0	0	0	0	1.07	83.49	15.44
22	157.76	357 000	0.3090	176.49	0	0	0	0	1	78.20	20.80
23	15.00	101 325	0.0007	32.93	0	0	100	0	0	0	0
24	133.20	368 000	0.0007	311.70	0	0	100	0	0	0	0
25	673.00	348 000	1.2951	1 062.21	0	2.86	0	0	16.51	68.20	12.43
26	470.08	108 000	1.2951	811.04	0	2.86	0	0	16.51	68.20	12.43
27	281.15	104 000	1.2951	587.81	0	2.86	0	0	16.51	68.20	12.43
28	122.55	101 325	1.2951	407.21	0	2.86	0	0	16.51	68.20	12.43

Table 15
Thermal results for the SOFC system at 650 °C.

	T[°C]	p[Pa]	ṁ[kg/s]	h[kg/s]	CO[%]	CO_2[%]	CH_4[%]	H_2[%]	H_2O[%]	N_2[%]	O_2[%]
1	15.00	101 325	0.0210	32.93	0	0	100.00	0	0	0	0
2	133.20	368 000	0.0210	311.70	0	0	100.00	0	0	0	0
3	15.00	101 325	0.0848	63.02	0	0	0	0	100.00	0	0
4	15.03	476 000	0.0848	63.49	0	0	0	0	100.00	0	0
5	180.00	368 000	0.0848	2 820.51	0	0	0	0	100.00	0	0
6	169.07	368 000	0.1058	2 322.73	0	0	21.75	0	78.25	0	0
7	291.44	361 000	0.1058	2 596.41	0	0	21.75	0	78.25	0	0
8	744.60	357 000	0.1058	3 240.19	7.68	6.89	0.85	50.58	34.00	0	0
9	650.00	350 000	0.1058	2 966.52	7.68	6.89	0.85	50.58	34.00	0	0
10	685.00	349 000	0.1676	2 949.24	0.73	13.83	0.85	12.09	72.49	0	0
11	15.00	101 325	0.8131	15.48	0	0	0	0	1.00	78.20	20.80
12	157.76	357 000	0.8131	176.49	0	0	0	0	1.00	78.20	20.80
13	157.76	357 000	0.6749	176.49	0	0	0	0	1.00	78.20	20.80
14	464.91	351 000	0.6749	502.76	0	0	0	0	1.00	78.20	20.80
15	650.00	350 000	4.1495	714.92	0	0	0	0	1.08	84.07	14.85
16	685.00	349 000	4.0878	756.13	0	0	0	0	1.09	85.20	13.71
17	685.00	349 000	0.6132	756.13	0	0	0	0	1.09	85.20	13.71
18	912.82	347 000	0.7807	1 601.06	0	4.44	0	0	25.64	62.25	7.68
19	815.18	343 000	0.7807	1 464.58	0	4.44	0	0	25.64	62.25	7.68
20	0	0	0	0	0	0	0	0	0	0	0
21	685.00	349 000	3.4746	756.13	0	0	0	0	1.09	85.20	13.71
22	157.76	357 000	0.1382	176.49	0	0	0	0	1.00	78.20	20.80
23	0	0	0	0	0	0	0	0	0	0	0
24	0	0	0	0	0	0	0	0	0	0	0
25	734.02	348 000	0.9190	1 270.82	0	3.82	0	0	22.18	64.48	9.52
26	523.50	108 000	0.9190	997.10	0	3.82	0	0	22.18	64.48	9.52
27	330.08	104 000	0.9190	757.48	0	3.82	0	0	22.18	64.48	9.52
28	114.99	101 325	0.9190	502.95	0	3.82	0	0	22.18	64.48	9.52

and 650 °C, respectively.

On the other side, the SOFC/MGT configuration does not require any amount of CO_2 in the oxygen electrode. It is only fed with air to satisfy the reactions involved in the SOFC stack. The CO_2 and H_2O in the oxygen electrode can be harmful for the operation of the cell decreasing its operative lifetime, which is the reason for avoiding gas recirculation in the oxygen electrode. The CO_2 leaving the fuel electrode increases because of the water–gas shift and steam reforming reactions that take place in the electrode. It increases again when leaving the catalytic burner, once the fuel is completely oxidized. The amount of CO_2 does not change when it crosses the reformer because only heat transfer occurs here. Then, the carbon dioxide flows to the auxiliary combustion chamber where some extra fuel can be supplied to meet the energy demands upstream. Fig. 12 shows the flow of CO_2 in the SOFC/MGT system. The annual amount of CO_2 expelled to the environment is 443.61 kg/year and 429.02 kg/year at 600 °C and 650 °C, respectively. These concluding results indicate that CO_2 emissions between these configurations are still lower in the SOFC/MGT system. Table 11

Table 16
Exergy results for the MCFC system at 600 °C.

	s[kJ/(kg•K)]	b_{th}[kJ/kg]	b_{ch}[kJ/kg]	b[kJ/kg]	B[kJ]
1	11.53	−0.01	51848.50	51848.49	1088.82
2	11.67	238.40	51848.50	52086.90	1093.83
3	0.22	0.00	49.96	49.96	4.24
4	0.23	0.37	49.96	50.33	4.27
5	10.64	769.76	49.96	819.72	69.55
6	11.10	590.54	10326.69	10917.24	1155.48
7	11.95	799.39	10326.69	11126.09	1177.59
8	16.24	1419.06	11907.20	13326.26	1410.45
9	15.78	1100.00	11907.20	13007.21	1376.68
10	8.82	676.38	1458.56	2134.94	690.62
11	6.89	0.00	4.53	4.53	5.53
12	6.94	147.68	4.53	152.22	185.72
13	6.94	147.68	4.53	152.22	163.44
14	7.45	282.68	4.53	287.22	308.39
15	8.18	443.73	30.05	473.78	1965.93
16	8.31	478.64	20.36	499.00	1962.00
17	8.31	478.64	20.36	499.00	1373.40
18	8.44	539.24	41.72	580.96	1786.92
19	8.39	505.31	41.72	547.03	1682.55
20	8.40	513.56	41.72	555.28	1707.92
21	8.31	478.64	20.36	499.00	588.60
22	6.94	147.68	4.53	152.22	22.29
23	11.53	−0.01	51848.50	51848.49	127.96
24	11.67	238.53	51848.50	52087.03	128.55
25	8.32	505.91	19.83	525.74	698.41
26	8.38	238.14	19.83	257.97	342.70
27	8.04	108.34	19.83	128.17	170.26
28	7.67	37.93	19.83	57.76	76.73

Table 17
Exergy results for the MCFC system at 650 °C.

	s[kJ/(kg•K)]	b_{th}[kJ/kg]	b_{ch}[kJ/kg]	b[kJ/kg]	B[kJ]
1	11.53	−0.01	51848.50	51848.49	1088.82
2	11.67	238.40	51848.50	52086.90	1093.83
3	0.22	0.00	49.96	49.96	4.24
4	0.23	0.37	49.96	50.33	4.27
5	10.64	769.76	49.96	819.72	69.55
6	11.10	590.54	10326.69	10917.24	1155.48
7	11.65	705.95	10326.69	11032.64	1167.70
8	16.17	1392.09	11881.39	13273.48	1404.87
9	15.90	1195.70	11881.39	13077.09	1384.08
10	9.04	738.15	1645.98	2384.14	743.10
11	6.89	0.00	4.53	4.53	6.57
12	6.94	147.68	4.53	152.22	220.68
13	6.94	147.68	4.53	152.22	189.79
14	7.57	334.87	4.53	339.40	423.18
15	8.19	477.65	26.89	504.54	2093.61
16	8.31	507.29	17.81	525.10	2070.80
17	8.31	507.29	17.81	525.10	1360.51
18	8.48	592.98	39.55	632.53	1836.01
19	8.42	545.09	39.55	584.64	1697.00
20	8.42	553.83	39.55	593.38	1722.37
21	8.31	507.29	17.81	525.10	710.28
22	6.94	147.68	4.53	152.22	30.90
23	11.53	−0.01	51848.50	51848.49	167.63
24	11.67	238.53	51848.50	52087.03	168.40
25	8.30	524.33	17.42	541.75	844.53
26	8.35	266.56	17.42	283.98	442.69
27	7.93	92.28	17.42	109.70	171.01
28	7.61	33.74	17.42	51.16	79.75

Table 18
Exergy results for the SOFC system at 600 °C.

	s[kJ/(kg•K)]	b_{th}[kJ/kg]	b_{ch}[kJ/kg]	b[kJ/kg]	B[kJ]
1	11.53	−0.01	51848.50	51848.49	1088.82
2	11.67	238.40	51848.50	52086.90	1093.83
3	0.22	0.00	49.96	49.96	4.24
4	0.23	0.37	49.96	50.33	4.27
5	10.64	769.76	49.96	819.72	69.55
6	11.10	590.54	10326.69	10917.24	1155.48
7	11.89	779.93	10326.69	11106.63	1175.53
8	16.17	1392.39	11881.70	13274.09	1404.93
9	15.74	1098.90	11881.70	12980.61	1373.87
10	11.26	992.23	2017.77	3010.00	505.32
11	6.89	0.00	4.53	4.53	5.39
12	6.94	147.68	4.53	152.22	180.92
13	6.94	147.68	4.53	152.22	133.88
14	7.51	309.92	4.53	314.45	276.57
15	7.70	407.24	4.90	412.14	1710.16
16	7.75	434.61	5.17	439.77	1797.56
17	7.75	434.61	5.17	439.77	359.51
18	8.66	668.56	24.51	693.07	682.93
19	8.58	605.54	24.51	630.05	620.83
20	0.00	0.00	0.00	0.00	0.00
21	7.75	434.61	5.17	439.77	1438.05
22	6.94	147.68	4.53	152.22	47.04
23	11.53	−0.01	51848.50	51848.49	37.02
24	11.67	238.40	51848.50	52086.90	37.19
25	8.32	505.62	19.08	524.69	679.54
26	8.38	237.81	19.08	256.89	332.70
27	8.05	110.94	19.08	130.02	168.39
28	7.67	38.13	19.08	57.21	74.09

Table 19
Exergy results for the SOFC system at 650 °C.

	s[kJ/(kg•K)]	b_{th}[kJ/kg]	b_{ch}[kJ/kg]	b[kJ/kg]	B[kJ]
1	11.53	−0.01	51848.50	51848.49	1088.82
2	11.67	238.40	51848.50	52086.90	1093.83
3	0.22	0.00	49.96	49.96	4.24
4	0.23	0.37	49.96	50.33	4.27
5	10.64	769.76	49.96	819.72	69.55
6	11.10	590.54	10326.69	10917.24	1155.48
7	11.65	705.84	10326.69	11032.53	1167.68
8	16.17	1391.92	11881.21	13273.13	1404.83
9	15.90	1195.69	11881.21	13076.90	1384.06
10	11.39	1065.10	2049.22	3114.33	521.86
11	6.89	0.00	4.53	4.53	3.69
12	6.94	147.68	4.53	152.22	123.77
13	6.94	147.68	4.53	152.22	102.73
14	7.51	308.43	4.53	312.96	211.22
15	7.77	446.97	5.34	452.31	1876.86
16	7.81	475.36	5.75	481.11	1966.66
17	7.81	475.36	5.75	481.11	295.00
18	8.93	794.59	31.65	826.23	645.07
19	8.82	691.65	31.65	723.29	564.70
20	0.00	0.00	0.00	0.00	0.00
21	7.81	475.36	5.75	481.11	1671.66
22	6.94	147.68	4.53	152.22	21.04
23	0.00	0.00	0.00	0.00	0.00
24	0.00	0.00	0.00	0.00	0.00
25	8.59	591.65	26.41	618.05	567.97
26	8.65	301.02	26.41	327.43	300.89
27	8.32	157.13	26.41	183.54	168.67
28	7.81	49.75	26.41	76.16	69.98

presents a summary of the thermal, economic, and environmental features of MCFC/MGT and SOFC/MGT systems at 600 °C and 650 °C.

5. Conclusions

A thermoeconomic comparison of a MCFC/MGT and a SOFC/MGT has been carried out in order to evaluate the best option to produce electricity. The systems were evaluated under the same operating conditions using the first-law of thermodynamics to size the components. The capacity of the fuel cell stacks was maintained at 500kW$_{dc}$ operating at 350 kPa and 600 °C/650 °C. The results indicate that the MCFC stacks are more efficient than the SOFC stacks at both analyzed temperatures. An exergetic analysis was carried out to assess the components and identify the main irreversibilities. The results indicate that the catalytic burner and the fuel cell stack are the components in both systems with the highest irreversibilities owing to the chemical reactions

that increase entropy generation. The SOFC/MGT system shows the highest overall efficiency. An economic analysis is also carried out to estimate the Levelized Cost of Electricity and to determine which is the most feasible option from an economic perspective. Although MCFC stacks are more efficient than SOFC stacks, these are considerably more expensive, with a PEC 4.9–6.4 times higher. The TCI of the MCFC/MGT system is 2.5–3.5 times higher than the SOFC/MGT system, so that produced electricity, which is the only product considered in the systems, is more expensive. Thus, the LCOE for the SOFC/MGT system is 0.339–0.402$/kWh and for the MCFC/MGT system is 0.875–0.897 $/kWh, though in both cases this is still higher than current electricity prices. The high price of fuel cell stacks contributes significantly to increasing the LCOE, although such price depends on external factors as well, such as e.g. the number of units produced per year: with increasing demand, more cost-effective production processes can be put in place and the price would be more accessible. MCFC are devices that can produce electricity and at the same time work as carbon capture devices. This is a feature of MCFC stacks that can contribute to mitigate the high TCI by decreasing the price in the main product and considering other delivered products as captured CO_2.

CRediT authorship contribution statement

Juan Pedro Pérez-Trujillo: Conceptualization, Methodology, Software, Validation, Writing - original draft. **Francisco Elizalde-Blancas:** Software, Validation, Writing - review & editing. **Massimiliano Della Pietra:** Methodology, Writing - review & editing. **Dulce María Silva-Mosqueda:** Validation, Writing - review & editing. **Juan Manuel García Guendulain:** Validation, Writing - review & editing. **Stephen J. McPhail:** Methodology, Writing - review & editing.

Declaration of Competing Interest

The authors declare that they have no known competing financial interests or personal relationships that could have appeared to influence the work reported in this paper.

Data availability

Data will be made available on request.

Appendix A

See Tables 12–19.

References

[1] Arsalis A. Thermoeconomic modeling and parametric study of hybrid SOFC–gas turbine–steam turbine power plants ranging from 1.5 to 10MWe. J Power Sources 2008;181:313–26. https://doi.org/10.1016/j.jpowsour.2007.11.104.

[2] Santin M, Traverso A, Magistri L, Massardo A. Thermoeconomic analysis of SOFC-GT hybrid systems fed by liquid fuels. Energy 2010;35:1077–83. https://doi.org/10.1016/j.energy.2009.06.012.

[3] El-Emam RS, Dincer I. Energy and exergy analyses of a combined molten carbonate fuel cell – gas turbine system. Int J Hydrogen Energy 2011;36:8927–35. https://doi.org/10.1016/j.ijhydene.2011.04.228.

[4] Minutillo M, Perna A, Jannelli E. SOFC and MCFC system level modeling for hybrid plants performance prediction. Int J Hydrogen Energy 2014;39:21688–99.

[5] Lee YD. Thermodynamic, economic and environmental evaluation of solid oxide fuel cell hybrid power generation systems. Technische Universitaet Berlin; 2015. https://doi.org/10.14279/depositonce-4546.

[6] Iora P, Campanari S, Salogni A. Off-design analysis of a MCFC-gas turbine hybrid plant. J Fuel Cell Sci Technol 2010;7. https://doi.org/10.1115/1.4000679.

[7] Ryu J-Y, Ko A, Park S-H, Park J-P. Thermo-economic assessment of molten carbonate fuel cell hybrid system combined between individual sCO2 power cycle and district heating. Appl Therm Eng 2020;169. https://doi.org/10.1016/j.applthermaleng.2020.114911.

[8] Scataglini R, Wei M, Mayyas A, Chan SH, Lipman T, Santarelli M. A direct manufacturing cost model for solid-oxide fuel cell stacks. Fuel Cells 2017;17:825–42. https://doi.org/10.1002/fuce.201700012.

[9] Ismail MS, Moghavvemi M, Mahlia TMI. Current utilization of microturbines as a part of a hybrid system in distributed generation technology. Renew Sustain Energy Rev 2013;21:142–52. https://doi.org/10.1016/j.rser.2012.12.006.

[10] Cigolotti V, Genovese M, Fragiacomo P. Comprehensive review on fuel cell technology for stationary applications as sustainable and efficient poly-generation energy systems. Energies (Basel) 2021;14:4963. https://doi.org/10.3390/en14164963.

[11] Mojaver P, Chitsaz A, Sadeghi M, Khalilarya S. Comprehensive comparison of SOFCs with proton-conducting electrolyte and oxygen ion-conducting electrolyte: thermoeconomic analysis and multi-objective optimization. Energy Convers Manag 2020;205:112455. https://doi.org/10.1016/j.enconman.2019.112455.

[12] Chen Y, Wang M, Liso V, Samsatli S, Samsatli NJ, Jing R, et al. Parametric analysis and optimization for exergoeconomic performance of a combined system based on solid oxide fuel cell-gas turbine and supercritical carbon dioxide Brayton cycle. Energy Convers Manag 2019;186:66–81. https://doi.org/10.1016/j.enconman.2019.02.036.

[13] Roy D, Samanta S, Ghosh S. Thermo-economic assessment of biomass gasification-based power generation system consists of solid oxide fuel cell, supercritical carbon dioxide cycle and indirectly heated air turbine. Clean Technol Environ Policy 2019;21:827–45. https://doi.org/10.1007/s10098-019-01671-7.

[14] Mohsin I, Al-Attas TA, Sumon KZ, Bergerson J, McCoy S, Kibria MG. Economic and environmental assessment of integrated carbon capture and utilization. Cell Rep Phys Sci 2020;1:100104. https://doi.org/10.1016/j.xcrp.2020.100104.

[15] Desideri U, Proietti S, Sdringola P, Cinti G, Curbis F. MCFC-based CO2 capture system for small scale CHP plants. Int J Hydrogen Energy 2012;37:19295–303. https://doi.org/10.1016/j.ijhydene.2012.05.048.

[16] Samanta S, Ghosh S. A thermo-economic analysis of repowering of a 250 MW coal fired power plant through integration of Molten Carbonate Fuel Cell with carbon capture. Int J Greenhouse Gas Control 2016;51:48–55. https://doi.org/10.1016/j.ijggc.2016.04.021.

[17] Yang Z, Guo M, Wang N, Ma C, Wang J, Han M. A short review of cathode poisoning and corrosion in solid oxide fuel cell. Int J Hydrogen Energy 2017;42:24948–59. https://doi.org/10.1016/j.ijhydene.2017.08.057.

[18] Nielsen J, Mogensen M. SOFC LSM:YSZ cathode degradation induced by moisture: an impedance spectroscopy study. Solid State Ion 2011;189:74–81. https://doi.org/10.1016/j.ssi.2011.02.019.

[19] Bischoff M, Huppmann G. Operating experience with a 250 kWel molten carbonate fuel cell (MCFC) power plant. J Power Sources 2002;105:216–21. https://doi.org/10.1016/S0378-7753(01)00942-9.

[20] Stathopoulos P, Sleem T, Paschereit CO. Steam generation with stoichiometric combustion of H2/O2 as a way to simultaneously provide primary control reserve and energy storage. Appl Energy 2017;205:692–702. https://doi.org/10.1016/j.apenergy.2017.07.094.

[21] González-Gómez PA, Gómez-Hernández J, Briongos JV, Santana D. Thermo-economic optimization of molten salt steam generators. Energy Convers Manag 2017;146:228–43. https://doi.org/10.1016/j.enconman.2017.05.027.

[22] Moran MJ, Shapiro HN, Boettner DD, Bailey MB. Fundamentals of engineering thermodynamics. John Wiley & Sons; 2010.

[23] Wark K. Advanced thermodynamics for engineers. McGraw-Hill New York; 1995.

[24] Bergman TL, Incropera FP, Dewitt DP, Lavine AS. Fundamentals of heat and mass transfer. John Wiley & Sons; 2011.

[25] Perez Trujillo JP. Experimental and numerical study of Molten Carbonate Fuel Cells working in reversible mode. Universidad de Guanajuato; 2019. PhD, http://repositorio.ugto.mx/handle/20.500.12059/4620.

[26] Silva Mosqueda DM. Experimental study on the performance of a single SOFC during internal reforming. Master thesis, Universidad de Guanajuato; 2019. http://148.214.84.21/handle/20.500.12059/4638 (accessed April 4, 2022).

[27] Arato E, Audasso E, Barelli L, Bosio B, Discepoli G. Kinetic modelling of molten carbonate fuel cells: effects of cathode water and electrode materials. J Power Sources 2016;330:18–27. https://doi.org/10.1016/j.jpowsour.2016.08.123.

[28] Pérez-Trujillo JP, Elizalde-Blancas F, McPhail SJ, della Pietra M, Bosio B. Preliminary theoretical and experimental analysis of a Molten Carbonate Fuel Cell operating in reversible mode. Appl Energy 2020;263:114630. https://doi.org/10.1016/j.apenergy.2020.114630.

[29] Leonide A, Apel Y, Ivers-Tiffee E. SOFC modeling and parameter identification by means of impedance spectroscopy. ECS Trans 2009;19:81–109.

[30] Bejan A, Tsatsaronis G, Moran MJ. Thermal design and optimization. John Wiley & Sons; 1995.

[31] Tsatsaronis G, Cziesla F. Thermoeconomics. In: Encyclopedia of physical science and technology. Elsevier; 2003. p. 659–80. doi: 10.1016/B0-12-227410-5/00944-3.

[32] della Pietra M, McPhail SJ, Prabhakar S, Desideri U, Nam SW, Cigolotti V. Accelerated test for MCFC button cells: first findings. Int J Hydrogen Energy. 2016;41:18807–14. https://doi.org/10.1016/j.ijhydene.2016.07.021.

[33] Maghsoudi P, Sadeghi S. A novel economic analysis and multi-objective optimization of a 200-kW recuperated micro gas turbine considering cycle thermal efficiency and discounted payback period. Appl Therm Eng 2020;166:114644. https://doi.org/10.1016/j.applthermaleng.2019.114644.

[34] Sanaye S, Hajabdollahi H. Multi-objective optimization of shell and tube heat exchangers. Appl Therm Eng 2010;30:1937–45. https://doi.org/10.1016/j.applthermaleng.2010.04.018.

[35] Hamelinck CN, Faaij APC. Future prospects for production of methanol and hydrogen from biomass. J Power Sources 2002;111:1–22. https://doi.org/10.1016/S0378-7753(02)00220-3.

[36] Mehr AS, Mahmoudi SMS, Yari M, Chitsaz A. Thermodynamic and exergoeconomic analysis of biogas fed solid oxide fuel cell power plants emphasizing on anode and

cathode recycling: a comparative study. Energy Convers Manag 2015;105:596–606. https://doi.org/10.1016/j.enconman.2015.07.085.
[37] Ahmadi R, Pourfatemi SM, Ghaffari S. Exergoeconomic optimization of hybrid system of GT, SOFC and MED implementing genetic algorithm. Desalination 2017;411:76–88. https://doi.org/10.1016/j.desal.2017.02.013.
[38] Najafi B, Shirazi A, Aminyavari M, Rinaldi F, Taylor RA. Exergetic, economic and environmental analyses and multi-objective optimization of an SOFC-gas turbine hybrid cycle coupled with an MSF desalination system. Desalination 2014;334:46–59. https://doi.org/10.1016/j.desal.2013.11.039.
[39] International Energy Agency. Water-Energy Nexus; 2016. https://www.iea.org/reports/water-energy-nexus (accessed July 8, 2022).
[40] Hamed O, Alwashmi H, Alotaibi H. Thermoeconomic analysis of a power/water cogeneration plant. Energy 2006;31:2699–709. https://doi.org/10.1016/j.energy.2005.12.011.
[41] Milewski J, Discepoli G, Desideri U. Modeling the performance of MCFC for various fuel and oxidant compositions. Int J Hydrogen Energy 2014;39:11713–21. https://doi.org/10.1016/j.ijhydene.2014.05.151.
[42] Perez-Trujillo JP, Elizalde-Blancas F, della Pietra M, McPhail SJ. A numerical and experimental comparison of a single reversible molten carbonate cell operating in fuel cell mode and electrolysis mode. Appl Energy. 2018;226:1037–55. https://doi.org/10.1016/j.apenergy.2018.05.121.
[43] Cheng T-C, Huang T-Y, Chen C-F, Tseng C-J, Lee S-W, Chang J-K, et al. Analysis of an intermediate-temperature proton-conducting SOFC hybrid system. Int J Green Energy 2016;13:1640–7. https://doi.org/10.1080/15435075.2016.1171229.
[44] di Carlo A, Borello D, Bocci E. Process simulation of a hybrid SOFC/mGT and enriched air/steam fluidized bed gasifier power plant. Int J Hydrogen Energy 2013;38:5857–74. https://doi.org/10.1016/j.ijhydene.2013.03.005.
[45] Duan L, Yue L, Feng T, Lu H, Bian J. Study on a novel pressurized MCFC hybrid system with CO 2 capture. Energy 2016;109:737–50. https://doi.org/10.1016/j.energy.2016.05.074.